Journal of Physics D:
Applied Physics

PAPER • **OPEN ACCESS**

Advancing plasma seed disinfection using a large-area pulsed wire-plate dielectric barrier discharge

To cite this article: L F A Wymenga *et al* 2026 *J. Phys. D: Appl. Phys.* **59** 295202

IOP Publishing J. Phys. D: Appl. Phys. 59 (2026) 295202 https://doi.org/10.1088/1361-6463/ae8b00

Journal of Physics D: Applied Physics

OPEN ACCESS

RECEIVED
22 May 2026

REVISED
29 June 2026

ACCEPTED FOR PUBLICATION
15 July 2026

PUBLISHED
23 July 2026

PAPER

Advancing plasma seed disinfection using a large-area pulsed wire-plate dielectric barrier discharge

L F A Wymenga[1,*], J van Turnhout[2], M Ghaffarian Niasar[3], H W van Zeijl[1], W D van Driel[1] and G Q Zhang[1]

[1] Electrical Components, Technology and Materials, Delft University of Technology, Delft, The Netherlands
[2] Materials Science and Engineering, Delft University of Technology, Delft, The Netherlands
[3] High Voltage Technologies, Delft University of Technology, Delft, The Netherlands
[*] Author to whom any correspondence should be addressed.

E-mail: l.f.a.wymenga@tudelft.nl, j.vanturnhout@tudelft.nl, m.ghaffarianniasar@tudelft.nl and willem.vandriel@tudelft.nl

Keywords: seed disinfection, inactivation, plasma agriculture, pulsed, dielectric barrier discharge, *Xanthomonas*, *Alternaria*

Supplementary material for this article is available online

Abstract

Seed production is a vital part of the global food supply chain. Seed surfaces are often contaminated with pathogenic fungal spores and bacteria, which cause plant diseases during germination. These pathogens prevent healthy crop growth and reduce yields by up to 40% in major crops. The future use of pesticides will be restricted by increasingly stringent regulations, while the demand for healthy crops continues to rise. Therefore, there is a growing need for eco-friendly technologies to inactivate seed-borne pathogenic microorganisms, without compromising seed quality. Cold atmospheric plasma (CAP) offers a promising alternative. Generated in ambient air, CAP is an ionized gas containing electrons, photons, ions, and reactive oxygen and nitrogen species (RONS). It does not leave toxic residues. Although CAP has demonstrated effective microbial inactivation at laboratory scale, its industrial implementation remains limited due to challenges in scalability, reliability and heat production. In this study, these limitations are addressed by developing and optimizing a wire-plate dielectric barrier discharge (DBD) for CAP seed disinfection, powered by high voltage pulses. The seed disinfection efficacy of the DBD was evaluated for cabbage and carrot seeds contaminated with bacteria (*Xanthomonas campestris* pv. *campestris* (Xcc) and *Xanthomonas hortorum* pv. *carotae* (Xhc)) and fungal spores (*Alternaria brassicicola*). Key parameters (such as treatment time, operating voltage and seed positioning) were investigated. The individual contribution of several plasma components (such as accelerated ions, RONS, pulsed electric fields) to seed disinfection was examined. Our results demonstrate that a large-area pulsed wire-plate DBD can achieve effective disinfection, while no reduction in seedling growth was observed. This highlights its potential as a scalable and sustainable alternative to conventional seed disinfection methods.

1. Introduction

There is an ongoing arms race between humans and pathogenic microorganims (viruses, bacteria, fungi and parasites). This struggle has led to the discovery of many disinfection strategies, such as cooking, pasteurization, pesticides and antibiotics [1]. Preventive measures such as sewerage, soap, sanitation and proper ventilation have saved millions of lives.

Many challenges however persist, such as the control and eradication of crop diseases [2]. Historically, plant diseases have had profound societal and economic impacts. A notable example is the extinction of the Gros Michel banana in the 1950's, caused by the fungus *Fusarium oxysporum*. Its successor, the Cavendish banana, now is the global monoculture banana. But since 2010, this banana is also being attacked by a new virulent strain of *Fusarium* (TR4). Another tragic example is the Great

Famine in Ireland (1845–1852). A parasite (*Phytophthora infestans*) infection of potatoes resulted in a catastrophic 90% yield loss and the deaths of around 1 M people.

Pathogenic bacteria and fungi reside in a dormant state mainly on the crop seed surface. Once the seed germinates, the pathogen becomes active and starts to grow, damaging the seedling and plant [3]. An example of such a disease is the black spot disease, caused by fungal *Alternaria brassicicola* spores on the seed surface [4]. *A. brassicicola* spores are quite resistant to environmental stressors (such as UV-light and oxidants) due to a protective, melanin-rich cell wall [3, 5]. In severe cases, *Alternaria* infections resulted in a yield loss of 86% in cabbage [6]! Bacterial pathogens also pose significant threats. The Gram-negative bacterium *Xanthomonas campestris* pv. *campestris*, or Xcc, causes black rot disease [7, 8]. It is one of the most destructive diseases affecting cabbage, carrot, rice and lettuce [9]. Another strain, *Xanthomonas hortorum* pv. *carotae* (Xhc), causes major yield losses in carrots by affecting the whole plant from root to leaves [10].

Conventional thermal disinfection methods (such as steam or hot water treatments and pasteurization) often impair seed viability and food quality [11]. This has driven the interest in non-thermal methods [12]. A comparison of non-thermal treatments is presented in [11]. Cold atmospheric plasma (CAP) has emerged as promising non-thermal technology for seed disinfection [13, 14]. It is an ionized gas, at or near ambient temperature and pressure, containing electrons, ions, reactive nitrogen and oxygen species (RNS and ROS, together reactive oxygen and nitrogen species (RONS)) and (UV) light emission [11]. When CAP interacts with microorganisms, it can inactivate them through various chemical processes, without leaving harmful residues [1, 15, 16]. Unlike chemical pesticides, it does not degrade soil fertility, and it might mitigate the emergence of microbial resistance due to lower antibiotic usage [17, 18]. It is a 'dry' process (requiring no water) and is applicable to a broad spectrum of pathogens [12].

CAP can be produced with various plasma sources, such as a corona discharge, a dielectric barrier discharge (DBD) and a plasma jet [19, 20]. These devices are all powered by high voltages (pulsed, AC or DC). Despite its proven efficacy at a laboratory scale, CAP has yet to achieve widespread industrial implementation [21]. Key limitations include scalability [11], material durability [22], excessive heat production [18] and overall energy efficiency.

In this study, we present a novel DBD module based on a large wire array, designed to address these limitations. The DBD has an electrode length of 7 m and is powered by positive nano- and micropulses. Its electrical performance and ozone production were characterized in detail. Next, it was investigated if the DBD could disinfect cabbage and carrot seeds, containing *A. brassicicola* spores, Xcc and Xhc on their surfaces. The contribution of the individual CAP components (RONS, ions, electrons, UV-light and pulsed electric fields (PEFs)) to seed disinfection was examined [13]. Also, the effects of treatment time, plasma intensity and seed surface morphology were assessed.

2. Method

2.1. DBD design and build

Gold-plated tungsten wire (TKS, Japan, diameter $d_e = 60$ μm) was chosen as discharge electrode. This wire is widely used as corona wire in photocopiers. The 300 nm-thick gold plating improves conductivity and provides oxidation resistance [14]. Wires generally possess a much smoother surface than printed or machined electrodes, which promotes a more homogeneous distribution and higher number of microdischarges [23]. Tungsten wires can be spanned over long distances with minimal elongation, rendering them suitable for large-area plasma units. The wire was spanned between two stainless steel springs and guided by 38 nylon pulleys that were integrated into a laser-cut PMMA (polymethyl methacrylate) frame. It was wound 35 times across the frame in parallel tracks, resulting in a total electrode length of $n \times l_e = 35 \times 200 = 7000$ mm (see figures 1 and 2).

The parallel wires were spaced 5.5 mm apart and positioned in 80 μm-deep guiding ridges. It produced an active plasma area of $A_{plasma} = 200 \times 200$ mm^2 (see figure 3).

The frame was placed on top of a flat dielectric barrier (305 $\times$ 305 mm^2, thickness d_d), which in turn rested on an aluminium ground electrode of 220 $\times$ 220 mm^2 (see figure 2). Thus, the wire was suspended slightly above the dielectric barrier (creating an air gap d_g of $\sim$ 20 μm). Microdischarges formed on both sides of the wire, doubling the active electrode length to 14 m (see figure 3). A PMMA lid was placed on the frame to create a closed air environment in which the seeds were placed (having a volume of 200 $\times$ 200 $\times$ 10 mm^3; 0.4 l). Depending on the treatment configuration, seeds could be placed either on the dielectric barrier (between the discharge wires) or on the bottom of the PMMA enclosure, by turning the unit upside down (see figure 2).

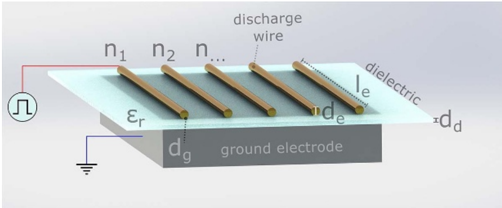

Figure 1. Setup of the wire-plate DBD. $n = 35$, ε_r: Dielectric barrier relative permittivity, $d_e = 0.06$ mm, $l_e = 200$ mm, d_d: Dielectric barrier thickness, $d_g \sim 0.02$ mm.

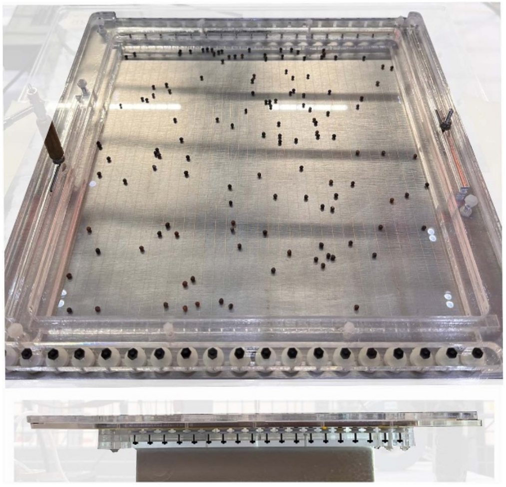

Figure 2. Top: DBD with cabbage seeds. Bottom: Side view of the DBD with PMMA lid, providing a closed treatment volume of 0.4 l. The DBD is placed in upside-down configuration (configure 2 in figure 8).

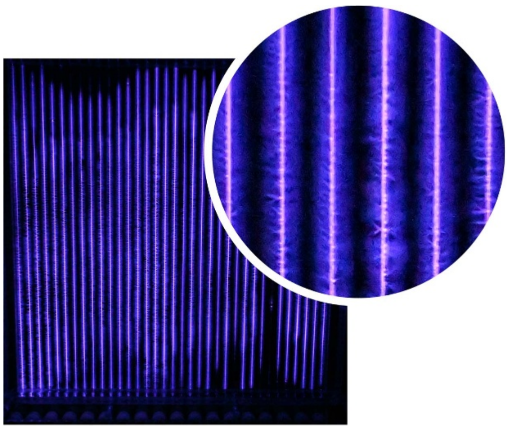

Figure 3. Microdischarge pattern during CAP production ($V_p = 3.0$ kV, PRF = 500 Hz, $t_{pulse} = 1$ μs, Gorilla glass barrier). The plasma area $A_{plasma} = 400$ cm^2.

To reduce the resistance of the long wire array, two additional Au–W wires were woven through the ends of the discharge wire near the pulleys, serving as shunts (see figure S1). This modification lowered the total resistance (spring-to-spring) from 120 to 10 Ω. It ensured that the applied voltage was delivered to all parallel wires simultaneously, without having to traverse the full 7 m wire length.

2.2. Dielectric barrier material selection

Several dielectric barriers were investigated. To enable large-scale CAP production, the following selection criteria were defined:

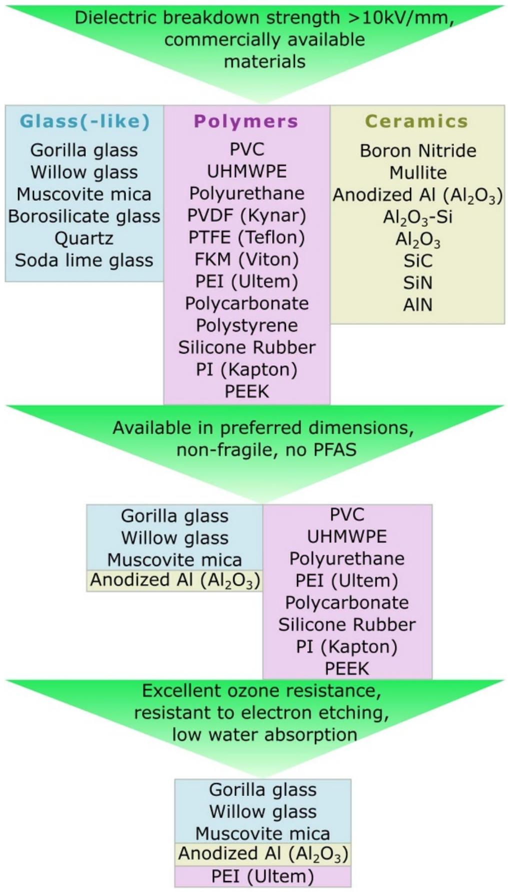

Figure 4. Flow chart for selection of dielectric barrier materials. Data is based on commercial availability (McMaster-Carr, USA [24]), material data sheets/databases [25–41] and literature [22, 42–51].

- Thickness $d_d \leqslant 0.5$ mm
- Dielectric breakdown strength >10 kV mm^{-1}
- Excellent ozone resistance (also in humid air)
- Low water absorption* (<1% weight/24 h)
- Surface area $\geqslant 250 \times 250$ mm^2
- Free of PFAS (per- and polyfluoroalkyl substances)
- Mechanically strong (non-fragile, resistant to plasma etching)
- Commercially available

*Some polymers may become more hydrophilic after plasma exposure

A decision flow chart based on these criteria is shown in figure 4.

Five barrier materials were selected based on this flow chart (see table 1 for details). These are Corning Willow flexible glass (processed alkali-free borosilicate), Corning Gorilla glass (processed alkali-aluminosilicate), Ultem polyetherimide (PEI, $C_{37}H_{24}O_6N_2$), muscovite mica ($KAl_2(AlSi_3O_{10})(OH)_2$) and alumina ($Al_2O_3$).

The ozone resistance of Willow glass and Gorilla glass is not known. However, because both consist primarily of glass oxides, we may expect excellent ozone resistance [25, 26].

Alumina is commercially available as thin sheets, but these are fragile and are only offered in small dimensions. An alternative route is to grow an alumina layer on aluminium through hard anodization [52], allowing large aluminium plates to be coated. Earlier research demonstrated successful CAP

Table 1. Dielectric barriers tested. DBS: Dielectric breakdown strength (for DC voltages). * A thicker PEI sheet ($d_d = 1.0$ mm) was applied first to evaluate its performance before the thin PEI film ($d_d = 25$ μm) was applied.

Material	ε_r	DBS (kV mm^{-1})	d_d (μm)
Willow glass	5.3	Unknown	100
Gorilla glass	6.8	Unknown	400
Ultem PEI	3.2	33	25*
Mica	6.0–8.0	100–200	100
Alumina	9.5–11.0	17–40	90
C-UHMWPE	Unknown	Unknown	100

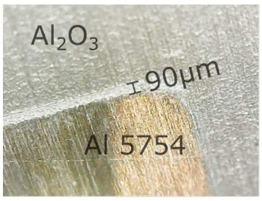

Figure 5. Detail of the aluminium (Al 5754) ground electrode, with the hard-anodized layer of alumina on top, acting as dielectric barrier.

production with two anodized aluminium electrodes, both having an Al_2O_3 coating of 120–250 μm thick [53, 54], although some alumina degradation was reported [55]. We used an Al 5754 plate (200 × 200 × 4 mm^3), which was hard anodized by the Alulox company (Schiedam, The Netherlands). This process forms a porous alumina layer of 90 μm thickness (see figure 5). The pores were subsequently sealed using a hot water treatment.

In addition to purely dielectric barriers, a partially conductive barrier was investigated, namely carbon-filled (2% volume) ultra-high molecular weight polyethylene (C-UHMWPE, see table 1). This resulted in a 'resistive barrier discharge', as described in [56]. The barrier had a surface resistivity of 105 Ω sq^{-1}. In resistive barrier discharges, surface charges decay faster than in a DBD due to the partial conductivity of the barrier. This mitigates distortion of the electric field due to surface charge accumulation (see section 3.3.1). However, the same effect suppresses the formation of secondary discharges (see section 3.3) [57].

2.3. Measurement setup

The experimental setup is shown in figure 6. The DBD is powered by a high-voltage push-pull switch (Behlke GHTS 100 A, with protective series resistor of 200 Ω). This switch delivers pulses with an adjustable peak voltage (V_p, 1–10 kV), pulse repetition frequency (PRF, 0–15 kHz) and pulse width (t_{pulse}, ⩾ 100 ns). The pulses have a rise time of ⩾23 ns, depending on the capacitive load of DBD [58]. The switch was powered by a positive DC high-voltage supply (Spellmann SL40PN600, 0–40 kV, 0–15 mA) which provided readouts of the DC voltage and current (V_{DC}, I_{DC}). The switch was triggered by a low-voltage pulse from a signal generator (Tektronix AFG3252C). The high-voltage pulses were measured at the switch output with a 1:1000 high-voltage probe (Tektronix P6015A with 10 ft. cable). The discharge current was measured at the ground side of the DBD with a current coil (Pearson 3525). In some of the experiments, an additional negative or positive DC supply (Spellman SL20PN150, 0–20 kV, 0–7.5 mA) was connected to a stainless steel grid (Maquett, 190 × 190 × 0.8 mm^3, mesh size 1.1 × 1.1 mm^2). This grid was used to accelerate ions towards the seeds.

Ozone concentrations were measured using a chemical ozone sensor (YuanTe Tech. Co. SKY2000-WH-O_3, 0–5000 ppm). The sensor has an internal pump and is calibrated at a flow rate of 0.6 l min^{-1} (see figure SA8). A Gerdien condenser ion metre (Alphalab Inc. AIC2), installed on top of a custom PMMA lid, was used to measure both positive and negative ion densities (see figure S2). Air temperature and relative humidity were measured with a handheld probe (Dostmann P670). Seed and barrier temperatures were recorded with an infrared thermometer (Fluke 68 IR). Capacitances were measured with an LCR metre (Keysight U1733C).

Photographs of the plasma were taken with a camera placed 100 mm above the barrier (Nikon Z7 II with Nikkor 24–120/4 S lense, shutter time 0.5 s, ISO25600). The DBD and camera were enclosed in a darkening tent (GlareOne LED Cube 60) covered with a blackout curtain. The camera was remotely

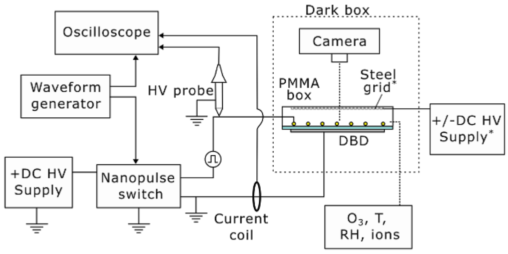

Figure 6. Schematic of experimental setup. * Only applied in part of the experiments, see figure 8.

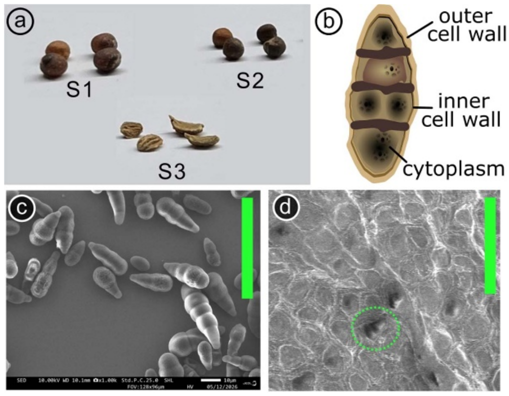

Figure 7. (a): Cabbage seeds (S1 and S2) and carrot seeds (S3) used in this study. (b): drawing of an *Alternaria* spore based on the microscopic observations in [59, 60]. (c): SEM image of *A. brassicicola* isolate from S1 seeds (bar height: 50 μm). (d): SEM image of a cabbage seed surface (S1) with a possible *A. brassicicola* spore encircled (magnification 650 $\times$ bar height: 100 μm).

operated using a wireless controller (CamRanger 2, with app). Scanning Electron Microscopy (SEM) was performed with either an electron beam energy of 3 keV (JEOL JSM-IT800 SHL, only figure 7(c)) or 2 keV (Philips XL30 SEFG, all other SEM images).

The signal generator output, the voltage probe signal and the current coil signal were monitored with a high-resolution oscilloscope (Rigol MSO5354, 350 MHz, 8 GSa s^{-1}). The current coil and waveform generator were connected to the oscilloscope with 50 Ω termination. All experiments were carried out in a grounded Faraday cage, with the researcher sitting outside the cage. Each measurement was repeated at least 3 times. Each voltage and current measurement represents the average of $\geqslant$64 pulses. An uncertainty analysis and calibration measurements are provided in the supplementary materials.

2.4. Seed treatment and analysis

Three types of dry, non-sterilized seeds were investigated (see figure 7(a)). The seeds were supplied by a Dutch seed company. We describe the seed treatment conditions following the protocol of Waskow *et al* [14]. S1 and S2 are spherical cabbage seeds, with diameters of around 2 and 1.5 mm, respectively. The surface of S1 seeds contained *A. brassicicola* spores and Xcc (see figures 7(b)–(d)), whereas S2 seeds contained Xcc. S3 are carrot seeds with an elongated shape and a rough surface containing many ridges and crevices, as observed in SEM (see figures S3 and S4). S3 contained Xhc on its surface. All seeds also carried many native, unidentified microorganisms.

For each treatment, $\sim$ 300 seeds (a mix of S1, S2 and S3) were placed inside the plasma reactor, which was gently shaken so that the seeds were not stacked on top of each other. The seed mix ensured that all seed types were exposed to the exact same ambient conditions per treatment. Earlier research by the seed company showed that the risk of cross-over contamination is negligible when using this method.

To assess the individual contributions of CAP components, the seeds were treated in four configurations (see figure 8). In configuration 1, the seeds rested on the barrier, between the discharge wires. They are then exposed to high densities of electrons, ions and RONS, as well as PEFs. In configuration 2, the seeds resided on the bottom of the PMMA box, 10 mm below the discharge wires. Here, the seeds are exposed to lower electron and ion densities compared to configuration 1, and no PEFs. Configuration 3 was identical to configuration 1, but with the PMMA chamber open. This allowed

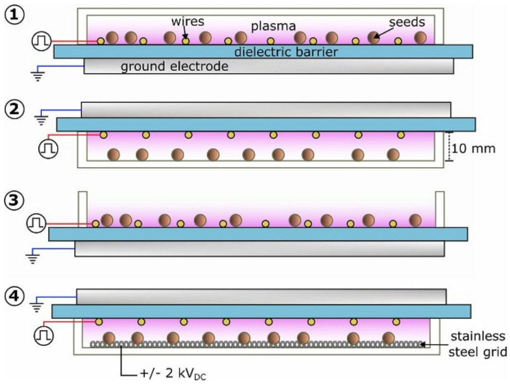

Figure 8. The four configurations of seed treatments. **1**: Seeds placed between the electrodes, closed box. **2**: Seeds placed 10 mm below the electrodes, closed box. **3**: Seeds between electrodes in open box. **4**: Seeds below electrodes, resting on a steel grid with a bias voltage of either +2 or−2 kV$_{\mathrm{DC}}$.

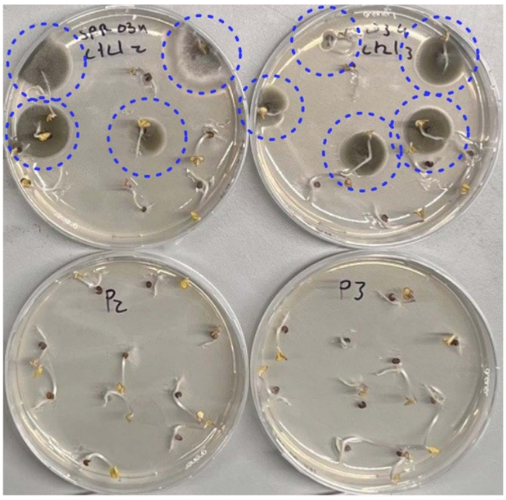

Figure 9. Four Petri dishes with containing 10 cabbage seeds (S2) each, photographed after 6 d. Top: untreated seeds. Bottom: treated seeds. Infected seeds are encircled in blue.

continuous exchange with ambient air, reducing the ion and RONS densities. In configuration 4, the seeds rested on a stainless steel grid, biased with a DC voltage of either 2 or −2 kV. A positive bias will accelerate negative ions (and electrons) towards the seeds, while repelling positive ions. A negative bias will accelerate positive ions, while repelling negative ions and electrons. The grid bias voltage did not affect the pulse shape and current waveform of the DBD (see figure S5), allowing the role of ions to be assessed selectively.

The treatment duration (t_{treat}) was 15–45 min, with $V_{\mathrm{p}} = 3$–4 kV, PRF = 500 Hz and $t_{\mathrm{pulse}} = 2$ μs. The ambient temperature was 20 ± 1 °C and the relative humidity was 42 ± 7% for all 24 experiments. Immediately after treatment, the PMMA box was opened. After a 'post-retention time' of 5 min, the seeds were transferred with tweezers onto sterilized Petri dishes (10 randomly picked seeds per dish) containing potato-dextrose agar medium (PDA, BD Difco, pH = 5.6). This is a non-selective medium, suitable for culturing both fungal and bacterial colonies, such as *Alternaria* and *Xanthomonas* [5]. To avoid cross-contamination, the tweezers were immersed in boiling water between plating the different seed types. The Petri dishes were sealed with laboratory film (Bemis Parafilm) and stored in a dark chamber for 6 d (under the same ambient conditions as during the experiments). After incubation, fungal and bacterial colonies could then be clearly observed around infected seedlings (see figure 9).

These colonies were counted to calculate the percentage of infected seeds. It should be emphasized that alongside the target pathogens, native microbial colonies could also grow on the medium. These were counted all together. Between treatments, the dielectric barrier, wire electrodes and container were cleaned with isopropyl alcohol. The barrier was flipped between each experiment to cancel the effect of

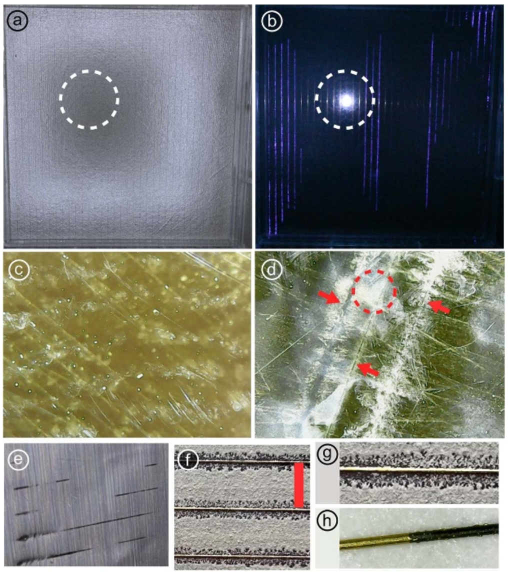

Figure 10. (a): Rigid mica sheet barrier covered with the discharge electrodes before CAP exposure. (b): Arcing (white circle) on the mica sheet when voltage was applied ($V_p = 2$ kV). (c): Ultem PEI barrier before CAP exposure ($d_d = 1$ mm). (d): Erosion (red arrows) and a white cloudy appearance along the discharge wires (red circle) were observed on the PEI barrier after CAP exposure. (e): Carbon-filled UHMWPE sheet exhibiting arcing damage. (f): Lycopodium powder visualization of microdischarge pattern on the Willow glass barrier ($V_p = 1.2$ kV, PRF = 500 Hz, $t_{pulse} = 1$ μs). Red bar height: 5.5 mm. (g): Magnification of the microdischarge pattern shown in figure 10(f). (h): Gold-plated tungsten wire after arcing, which destroyed the gold plating on the right end.

residual surface charges (see section 3.3.1). All seed experiments were performed with a Gorilla glass dielectric barrier.

3. Results

3.1. Dielectric barrier performance

Two types of mica barriers were tested, namely flexible and rigid mica. These showed sparks at $V_p = 1500$ and 2000 V, respectively (see figures 10(a) and (b)). This arcing suggests that these thin mica sheets could not withstand the high electric fields generated near the discharge wires.

The Ultem PEI sheet ($d_d = 1$ mm) showed visible damage already after 5 min of operation ($V_p = 4$ kV, PRF = 1000 Hz, $t_{pulse} = 3$ μs, see figures 10(c) and (d)). Ridges were observed on the barrier beneath the wire electrodes. This was most likely caused by plasma etching. Along the tracks, a white cloudy pattern appeared. This pattern remained after cleaning with isopropyl alcohol, indicating permanent material degradation. Thus, Ultem PEI is not resistant to CAP. Therefore, the Ultem PEI barriers (of both 1 and 0.025 mm thickness) were discarded.

The C-UHMWPE barrier also broke down rapidly. It produced sparks when $V_p > 1000$ V, resulting in severe damage of the C-UHMWPE sheet and the discharge wire itself, which had to be replaced (see figures 10(e) and (h)). This suggests that a resistive barrier discharge can only be used for CAP production when the air gap is sufficiently large.

The alumina barrier gave short circuits before CAP was formed at $V_p \sim 700$ V and was therefore also rejected. The sparking is likely due to microscopic defects (such as open pores in the anodized layer).

Willow glass and Gorilla glass barriers both demonstrated stable plasma production and incurred minimal damage. However, both barriers showed progressive surface charging over time, induced by the applied positive high-voltage pulses (see section 3.3.1).

3.2. Lycopodium powder pattern

The microdischarge pattern of a surface DBD could be visualized using powder particles [61, 62]. These are, depending on their charge, either attracted or repelled by the electric field emanating from the discharge wire.

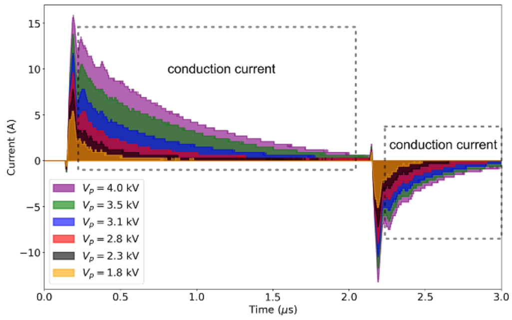

Figure 11. Current profiles for various pulse peak voltages (PRF = 500 Hz, $t_{pulse} = 2\ \mu$s, $T = 18.5\ ^\circ$C, RH = 40%). The regions where conduction current is present are highlighted. Average of 64 pulses.

We used Lycopodium spores with a diameter of $\sim 30\ \mu$m (Sigma-Aldrich 19 108–100 G–F) to visualize this. These carry a negative charge and enable visualization of the discharge locations. The powder was gently sieved on the barrier. The barrier was then tilted so that only a thin layer of powder remained. The wire electrodes were then gently placed on the barrier and high-voltage pulses were applied for 10 s. Clearly, distinct microdischarge footprints were observed on both sides of the wires (see figures 10(f) and (g)).

The streamer channels extended laterally along the dielectric barrier surface, in accordance with the light emission pattern shown in figure 3. Electric field interference between neighbouring wires may occur [63]. Therefore, sufficient wire spacing should be maintained.

3.3. VI-characteristics (Gorilla glass barrier)

To optimize operating conditions prior to seed disinfection, the voltage and current behaviour of our DBD with the Gorilla glass barrier was characterized. V_p was gradually increased, while monitoring the current waveform and light emission. The total measured current is generally expressed as the sum of the displacement current (I_{disp}) and the conduction current (I_{cond}) during plasma operation [64]:

$$I_{tot}(t) = I_{disp}(t) + I_{cond}(t). \tag{1}$$

During one pulse, a positive primary discharge and a negative secondary discharge were observed (see figure 11). The secondary discharge appears when positive surface charge, accumulated on the barrier, initiates a breakdown when the voltage pulse decays. Both discharges displayed an initial current peak, which is solely a displacement current when $V_p < 2$ kV (as then, no light emission or ozone production were observed). When $V_p > 2$ kV, conduction current appeared, as light emission and ozone production were observed (see figure 11 and section 3.4). The current profile showed the characteristic *two-peak* phenomenon as described in [64, 65]. The 'tails' of the primary and secondary discharge correspond to conduction current, associated with CAP formation (see figure 11). When $V_p = 3$ kV, microdischarges appeared on nearly all wires (see figure 3). So, $V_p \geqslant 3$ kV was selected for our seed treatment experiments.

The effect of pulse width was investigated by varying t_{pulse} between 500 and 3000 ns (see figure 12). We observed that the conduction current of the primary discharge lasted $\sim$1.5 μs. This relative long duration is attributed to the unusually long discharge electrode, which acts as a RC-circuit, with time constant τ = RC. Therefore, t_{pulse} should exceed 1.5 μs to ensure that microdischarges can form along the entire electrode length. As such, the pulse width for our seed experiments was set to $t_{pulse} = 2\ \mu$s.

Variation of the pulse repetition frequency showed no significant change in pulse current shape (see figure 13). However, the DC supply current increased from 0.6 to 10 mA when the PRF increased from 100 to 2000 Hz. Both C_{cell} (260 pF) and the plasma formation increased the capacitive load, which increased the rise time of the high-voltage pulse [58, 66, 67]. We found a rise time (10%–90%) of 750 ns when $V_p = 3$ kV.

3.3.1. Surface charging

A gradual decrease in conduction current was observed after 2 h of continuous CAP production (see figure 14). This behaviour was attributed to surface charging of the Gorilla glass barrier, which lowers the effective electric field in the air gap over time. Similar charging effects have been reported for a range of polymer barriers, such as Teflon, polyimide and polypropylene [68–71].

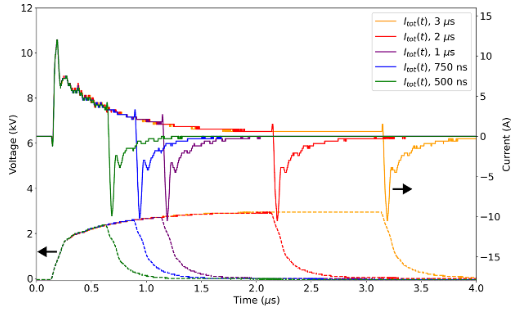

Figure 12. Voltage and current waveforms for $t_{\text{pulse}} = 500$–3000 ns (PRF = 500 Hz, $T = 21.5$ °C, RH = 52%). Average of 64 pulses.

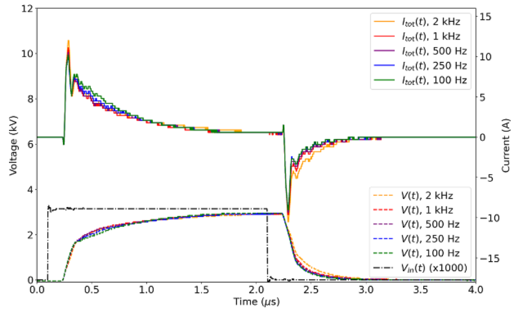

Figure 13. Current and voltage waveforms for varying PRF ($V_{\text{p}} = 3$ kV, $t_{\text{pulse}} = 2$ μs, $T = 21.5$ °C, RH = 52%). V_{in}: Low-voltage input pulse. Average of 64 pulses.

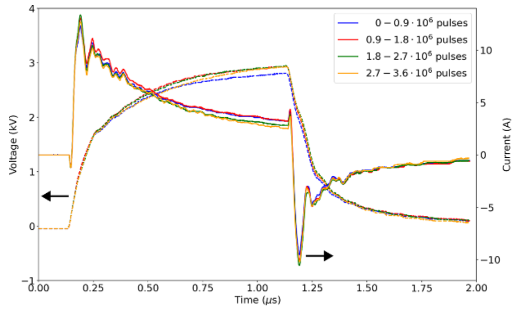

Figure 14. A small decrease in current was noticed after extended operation up to $3.6 \cdot 10^6$ pulses ($V_{\text{p}} = 3$ kV, $t_{\text{pulse}} = 1$ μs, PRF = 500 Hz). Average of 448 pulses.

Since Gorilla and Willow glass are insulating multi-component oxides, they are susceptible to charging and may retain charges for extended periods [25, 26]. Pipa *et al* noted that residual surface potentials influenced the breakdown voltage V_{br} for more than 13 h [72]. In the present study, a slight increase in V_{p} was required over time to maintain the same peak current (see figure 14).

To overcome this effect, the dielectric barrier was flipped between experiments, and both sides were cleaned with isopropyl alcohol to neutralize any charge retained on the barrier. After 30 min of operation, C_{cell} increased from 260 pF to 2.3 nF due to surface charging. Flipping and cleaning of the Gorilla glass barrier restored C_{cell} to its initial value, indicating complete removal of the surface charge. Therefore, no decrease in conduction current was observed between seed disinfection experiments (see figure 15). The Willow glass barrier ($d_{\text{d}} = 0.1$ mm) proved too fragile to flip and shattered. Therefore, all seed disinfection experiments were performed using the robust Gorilla glass barrier.

In an open PMMA box (configuration 3), the conduction current was consistently lower than in the closed box configurations (see figure 15). This was attributed to a lower ion density when the box is open: ions escape into the environment, thereby reducing the air conductivity (see also section 3.4). Placing seeds between the discharge wires (configure 1) did not affect the VI-characteristics, affirming that this placement did not alter the electrical behaviour of the DBD.

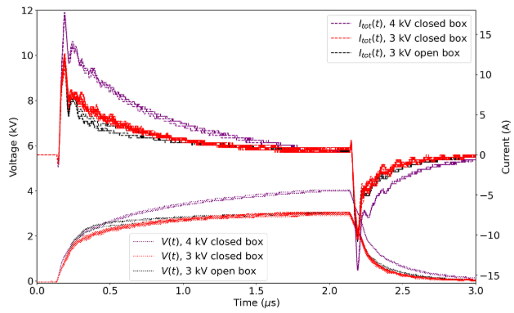

Figure 15. Current and voltage curves of all 24 seed treatments. No noticeable effect of surface charging was observed. The treatments with $V_p = 3$ kV represent 21 trials, totalling $18.9 \cdot 10^6$ pulses.

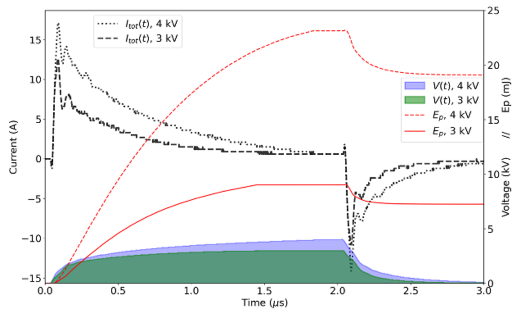

Figure 16. The energy per pulse E_p (red curves) for 3 and 4 kV pulses ($t_{pulse} = 2$ μs, PRF = 500 Hz).

3.3.2. Energy per pulse (E_p)

The energy per pulse E_p (in J) can be calculated by integrating the product of voltage and current over the duration T of a single pulse [73]:

$$E_p = \int_{T}^{0} V(t) \cdot I_{tot}(t)\,\mathrm{d}t. \tag{2}$$

The power P (in W) can then simply be obtained from E_p using:

$$P = \mathrm{PRF} \cdot E_p \tag{3}$$

Figure 16 shows E_p for 3 and 4 kV pulses, using equation (2). As expected, E_p increased with increasing pulse voltage, due to a greater number of microdischarges and increased streamer length. This is reflected in the larger conduction current at higher voltages in figures 11 and 16. We found $E_p = 7.3$ mJ for 3 kV pulses, and $E_p = 19.1$ mJ for 4 kV pulses. This corresponds to $P = 3.65$ and 9.55 W for 3 and 4 kV pulses, respectively, using equation (3). These values were used for subsequent energy calculations in section 3.5.

3.4. Ozone, temperature and ion production

Ozone production was monitored in configuration 1, using a PMMA lid with two holes serving as air inlet and outlet (see figure S6). The ozone metre was connected airtight to the air outlet. The results are presented in figure 17. Ozone levels increased rapidly when the plasma was formed, then approached saturation. Ozone levels increased with PRF, although not proportionally, consistent with previous observations [74]. Increasing the PRF from 500 to 2000 Hz increased the maximum ozone concentration $[O_3]_{max}$ by 59%. Increasing V_p from 3 to 4 kV raised $[O_3]_{max}$ by 30%. Reducing the humidity from 54%–28% (the difference between summer and winter day conditions) increased $[O_3]_{max}$ by 127%.

After 30 min of seed treatment, the seed and barrier temperature increased by only 2.0 and 3.3 °C above the ambient temperature of 19.6 °C ($V_p = 3$ kV, average of three measurements). After 45 min, the temperature increased by 3.8 and 4.9 °C, respectively. When $V_p = 4$ kV, the seed and barrier temperature reached 27 and 28 °C, respectively, far below heat-damage thresholds. These findings indicate that the seeds are neither disinfected nor damaged thermally and that the DBD operates in *ozone mode*

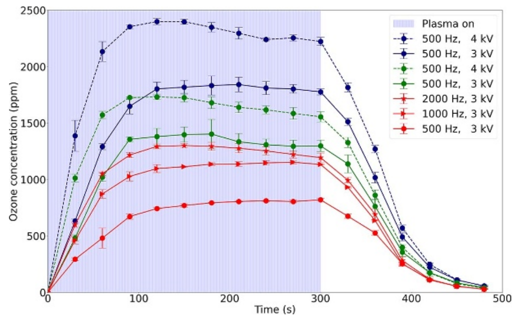

Figure 17. Ozone concentration for varying PRF, V_p and relative humidity ($t_{pulse} = 2\ \mu$s, $T = 18\ ^\circ$C–21 °C). Average of three measurements, standard deviations are displayed. Blue lines: RH = 28%. Green lines: RH = 44%. Red lines: RH = 54%.

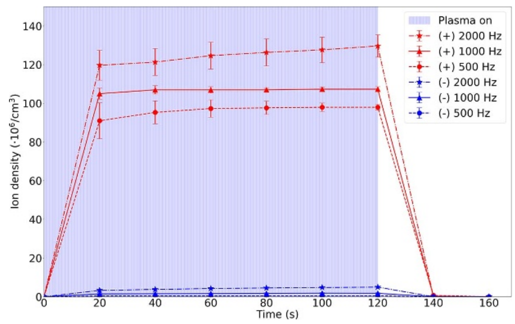

Figure 18. Positive and negative ion density for three PRFs ($V_p = 3$ kV, $t_{pulse} = 2\ \mu$s, $T = 22.8\ ^\circ$C, RH = 43%). Average of 3 measurements with standard deviations.

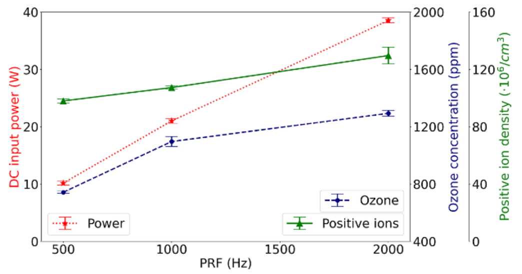

Figure 19. DC input power, ozone concentration and positive ion density (after 2 min. Operation) vs PRF ($V_p = 3$ kV, $t_{pulse} = 2\ \mu$s, $T = 20.8\ ^\circ$C–22.8 °C, RH = 43%–56%). Average of 3 (ozone, ions) and 8 (DC power) measurements. Standard deviations are displayed.

rather than in *NO_x mode* [75, 76]. This is important, because previous studies showed more effective inactivation of mycotoxins and *Aspergillus flavus* spores in ozone mode [77, 78].

Positive and negative ion densities were also measured as a function of PRF. As positive pulses were applied to the discharge electrodes, positive ions were expected to outnumber the negative ions. This was confirmed experimentally, see figure 18. Ion densities increased with PRF, but not proportionally [79]. During our treatments, the seeds were exposed to a positive ion density of 98 million per cm^3 and a negative ion density of 0.4 million per cm^3.

Notably, in the experiments with $-2\ kV_{DC}$ applied to the steel grid, the current of the DC supply providing this voltage increased by 0.03 mA during plasma operation. This was attributed to positive ions being attracted to the negatively charged grid. No such increase occurred for a $2\ kV_{DC}$ bias, because of the much lower density of negative ions. This is another confirmation of positive ions outnumbering negative ions in our setup.

In figure 19, $[O_3]_{max}$, the positive ion density and the DC input power ($V_{DC} \times I_{DC}$) are plotted as function of the PRF. While the DC power consumption increased linearly with PRF, ozone and ion production did not. Thus, the DBD became less energy-efficient for ozone and ion generation at higher PRF.

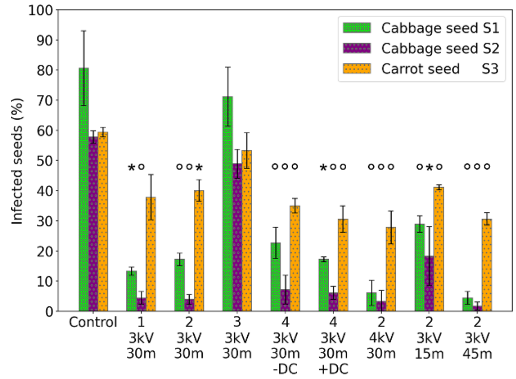

Figure 20. Percentage of infected seeds for each treatment. Each bar is the mean value of three measurements (60 seeds per measurement). Error bars show the standard deviations. The labels below the bars note the configuration number (see figure 8), V_p, treatment time and if a grid with DC bias was added, respectively. Statistically significant differences compared to control were calculated with one-tailed, paired t-tests in Excel. These were displayed by symbols above the treatments. *: $p < 0.05$, °: $p < 0.01$.

Table 2. Best disinfection results.

Seed	Control (%)	Best treatment (%)	Reduction
S1	81 ± 12	1.7	**98%**
S2	58 ± 2	0	**100%**
S3	59 ± 2	21.8	**63%**

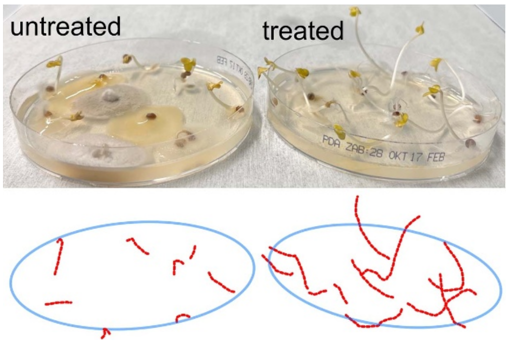

Figure 21. S2 seeds 9 d after plating. Left: untreated seeds. Right: treated seeds (configuration 2). The seedlings of the treated seeds showed longer stems compared to those of the untreated seeds. The stems are depicted in the bottom figure by drawing red lines over the stems visible in the photograph.

3.5. Disinfection of seed surfaces

The disinfection results for all seed types and configurations are shown in figure 20. The highest disinfection efficiencies were obtained with the 4 kV treatment (30 min) and the 3 kV treatment (45 min) in configuration 2.

The best results per seed type are summarized in table 2.

No reduction of seedling growth was observed. On the contrary, a higher number of seeds germinated after CAP treatment. The treated seeds clearly produced seedlings with longer stems (see figure 21). This could be explained by seed priming (a well-documented effect of CAP [80–83]) and/or by lower growth inhibition due to lower pathogenic microorganism activity [18]. Šrámková *et al* treated Saxon seeds and found that the increased germination power persisted after storage for up to 6 months [84]. Furthermore, improved growth was observed in plum plants even 3 years after CAP treatment at the seedling state [85].

The treatment in configuration 2 with $V_p = 3$ kV was conducted for several durations, as depicted in figure 20. These results were plotted with the treatment time on the x-axis in figure 22. A distinct time-dependent increase in disinfection efficiency was observed.

As our experiments were carried out under ambient laboratory conditions, natural variations in ambient temperature and relative humidity did occur. To evaluate their potential influence, the same

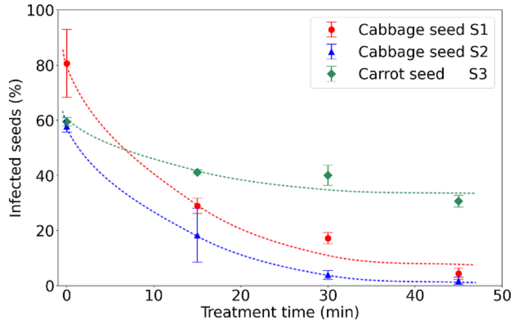

Figure 22. Percentage of infected seeds versus treatment time ($V_p = 3$ kV). The number of infected seeds appears to decay exponentially over time. Average of three measurements, standard deviations are displayed. Trendlines were drawn manually.

Table 3. Disinfection performance at two humidity levels (each treatment represents 60 seeds per seed type). The percentage of infected seeds after both treatments is given. Δ: Absolute difference in disinfection percentage between treatments.

Seed	RH = 36% $T = 19.1$ °C	RH = 49% $T = 20.2$ °C	Δ (%)
S1	5.0%	6.7%	1.7
S2	0.0%	1.7%	1.7
S3	28.3%	30.0%	1.7

Table 4. Energy and ozone characteristics of the 3 and 4 kV treatments. t_{treat}: Treatment time. $\#_{pulse}$: Total number of pulses per treatment. $[O_3]_{max}$: Maximum ozone concentration. E_{tot}: Total energy. E_{DC}: Total DC input energy. P_{dens}: power density.

V_p (kV)	t_{treat} (min)	$\#_{pulse}$	$[O_3]_{max}$ (ppm)	E_p (J)	E_{tot} (kJ)	E_{DC} (kJ)	P_{dens} (W cm^{-2})
3	45	$1.35 \cdot 10^6$	1403	$7.3{\cdot}10^{-3}$	9.9	26.5	0.009
4	30	$0.9{\cdot}10^6$	1732	$19.1{\cdot}10^{-3}$	17.2	44.5	0.024

treatments were repeated under different ambient conditions. The variations had no significant effect on the disinfection, see table 3.

Further analysis was performed on the 3 and 4 kV treatments that produced the highest disinfection percentages in figure 20. The total number of pulses ($\#_{pulse}$) and $[O_3]_{max}$ were determined. In addition, the total energy deposition ($E_{tot} = E_p \cdot \#_{pulse}$), DC energy use ($E_{DC} = V_{DC} \cdot I_{DC} \cdot 60{\cdot}t_{treat}$) and power density ($P_{dens} = P/A_{plasma}$) were calculated. These values are listed in table 4. It was found that E_{tot}, E_{DC} and P_{dens} were resp. 42, 40 and 63% lower for the 3 kV treatment than for the 4 kV treatment, despite its 50% longer treatment time. This is important, as the two treatments produced equally high disinfection rates.

4. Discussion

4.1. Seed disinfection mechanisms

4.1.1. Direct vs indirect treatment

No significant difference was observed between direct and indirect treatment (configuration 1 and 2). In a direct treatment, the seeds are exposed to PEFs, (relatively) high energized electron densities and UV emission, whereas these components are largely absent during indirect treatment [14, 21]. The lack of difference therefore indicates that these factors did not significantly contribute to seed disinfection. Instead, both configurations expose seeds to comparable RONS concentrations, which likely explains the similar disinfection percentages [77].

Several studies support the efficiency of indirect CAP treatments. Wannicke *et al* showed that *Bacillus atrophaeus* spores could be inactivated by plasma-treated air transported to the spores, without exposing them directly to the discharge [86]. Hertwig *et al* achieved indirect inactivation of *B. atrophaeus* and *Bacillus subtilis* spores on glass beads with a coplanar surface DBD [87].

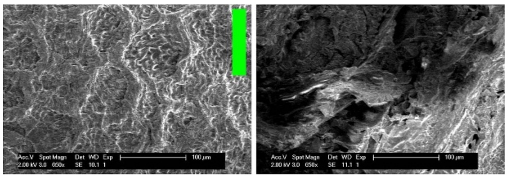

Figure 23. SEM images of the surface structure of a cabbage seed (left) and a carrot seed (right). Magnification 650 ×, bar height 100 μm.

Direct treatment has also been shown effective. Suwannarat *et al* inactivated *A. brassicicola* spores on kale seeds using a direct treatment [4]. Butscher *et al* observed degradation of *Geobacillus stearothermophilus* spores in a direct treatment, attributed primarily to chemical interaction with RONS [88]. Similar results were reported in [89], where several *Bacillus* and *Penicillium nalgiovense* spores were inactivated by a direct air plasma treatment.

Klämpfl *et al* inactivated *G. stearothermophilus* indirectly, as well as *Bacillus pumilus, B. subtilis* and *B. atrophaeus*, while UV-emission was blocked [90]. This aligns with the fact that UV-*B* and UV-*C* are heavily absorbed by oxygen and ozone in the air gap before reaching the spores (as is the case in configuration 2) [14]. Butscher *et al* found that strong varying electric fields did not contribute to the inactivation of *G. stearothermophilus* spores and *Escherichia coli* bacteria, consistent with our findings [88, 91].

Additionally, the low recorded seed temperature in our treatments exclude thermal inactivation (via IR radiation) as contributing mechanism [13]. Direct treatment inside an open PMMA box yielded no significant disinfection (see figure 20). The RONS and ion concentrations are then substantially reduced compared to a closed box. This supports the hypothesis that RONS are the primary agents responsible for microbial inactivation in our setup [92]. However, based on these findings, we cannot separate the contribution of individual RONS to this disinfection effect. The role of ions is discussed in the next section.

4.1.2. Ion bombardment

Placing the seeds on a biased steel grid (2 or −2 kV_{DC}) did not significantly improve disinfection (see figure 20). Thus, ion bombardment did not contribute substantially to seed disinfection [15]. Although a study reported on *B. atrophaeus* spore inactivation using a 100 eV ion beam (ion etching), this mechanism was clearly not active in our setup [93]. Some authors have suggested a synergistic effect between ion bombardment and RONS [13, 89, 91], but no such synergy was observed here. However, when ions are lost to the environment (as in configuration 3), the RONS concentration around the seeds will also decline, as RONS formation is dependent on the presence of ions.

4.1.3. Influence of seed surface

Disinfection efficacy was found to depend on seed type, with the spherical cabbage seeds (S1 and S2) showing higher disinfection rates than the irregularly shaped carrot seeds (S3). The latter possess a much rougher surface, with pronounced grooves, crevices and fissures (see figure 23). Such surface features enable microorganisms to penetrate deeper into regions of the seed coat, where they are better shielded from RONS exposure [77, 91, 94].

We did not detect a change in surface structure after CAP treatment (see SEM images in figures S3 and S4), indicating that the microtopography responsible for microbial protection remained intact. A similar substrate-dependent effect in CAP treatments was observed by Laika *et al* [77]. They found that the geometry of the substrate (whole versus chopped pistachios) affected the mycotoxin reduction. Likewise, Butscher *et al* found more rapid *E. coli* inactivation on smooth seeds (cress, alfalfa, radish) than on grooved seeds (onion) [91]. They also reported lower *G. stearothermophilus* inactivation on rougher surfaces [88], which they attributed to differences in electric field distribution (in a volume DBD) and/or seed stacking. Both explanations can be excluded in our setup, where the electric field was identical for all 3 kV treatments and seeds were arranged without stacking. Schnabel *et al* found lower plasma inactivation of *B. atrophaeus* endospores on cabbage seed surfaces compared to on glass substrates [94]. Similarly, Beyrer *et al* showed that *Bacillus coagulans* spores were much more effectively inactivated on flat glass substrates than in porous powder or maize starch [89]. They attributed the inactivation largely to ion-driven etching. However, our results show that accelerated ions do not boost the disinfection. Even without ion acceleration (i.e. in configuration 2), high disinfection was achieved. Furthermore, the

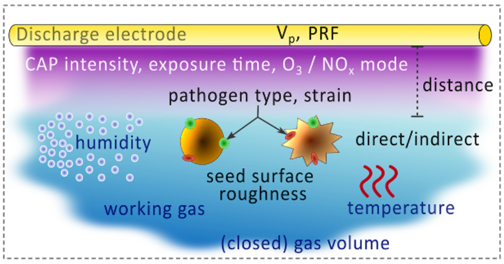

Figure 24. Factors which determine the success of CAP seed disinfection.

ions formed by nano- and micropulsed plasmas are barely accelerated compared to those formed by AC-powered plasmas.

Taken together, these findings suggest that rough surfaces hinder CAP disinfection primarily by limiting the accessibility of RONS to microorganisms. This may result from physical shielding or from interactions between RONS and the seed surface (such as scavenging or uptake processes [11, 13]).

4.1.4. Humidity

Variations in ambient humidity could not be avoided during our experiments. Large humidity variations could significantly alter CAP inactivation of microorganisms such as *Bacillus* spores and *Salmonella* bacteria [95, 96]. It can be explained by variations in radical formation. In dry air plasmas, strong disinfectants are singlet oxygen ($^1O_2$), superoxide (O_2^-) and ozone [21, 97]. In humid air plasmas, other strong oxidizers such as hydroxyl radicals (·OH), hydrogen peroxide (H_2O_2), HNO_3, ONOO- and HNO_2 appear, while the ozone concentration typically decreases (see figure 17) [97, 98]. Humidity may also change spore properties: it could cause swelling [99] or break spore dormancy [14]. The humidity variations encountered during our experiments did not significantly affect the disinfection efficacy (see table 3). This indicates that, in our experiments, the disinfection effect was not significantly increased by the mentioned humid air species. The disinfection could be explained by a sufficient high concentration of oxidizers such as ozone, singlet oxygen and superoxide over the entire humidity range of our experiments.

4.1.5. CAP intensity and exposure time

The CAP intensity (determined by V_p and PRF) and exposure time were found to be the most decisive factors deciding microorganism inactivation [87–91, 100]. This is schematically visualized in figure 24. A high voltage and/or PRF raise the concentration of RONS (wherein O_3 is the most abundant species) [78]. However, we found that prolonged exposure at somewhat lower $[O_3]_{max}$ achieved the same level of disinfection (see section 3.5). This suggests that for disinfection purposes, CAP devices and their power electronics should be designed to operate at moderate voltage (V_p slightly above V_{br}) and PRF. Under these conditions, ozone production is most energy efficient, while less heat is produced [101]. Treatment time could then be adjusted to obtain the desired disinfection effect. Our findings also indicate that increasing PRF is an inefficient strategy to enhance ozone production. This is likely due to surface charge accumulation on the dielectric barrier, which changes the local electric field and hinders further discharge development [102]. A high PRF could also increase the microdischarge channel temperature up to a point where ozone is thermally dissociated.

Supporting the above, Dasan *et al* showed that the treatment time had a greater impact on the inactivation of *Aspergillus* spores on hazelnuts than the operating voltage [103]. Yoshino *et al* demonstrated a clear time-dependent inactivation of *Aspergillus niger* and *B. subtilis* spores on steel Petri dishes in an oxygen low-pressure plasma. However, no *A. niger* inactivation occurred below a threshold plasma intensity (50 W), suggesting that a minimum intensity is required to overcome spore resistance to RONS [104]. Importantly, a too low CAP intensity might stimulate spore germination [105]! This highlights the need for careful optimization of the operating conditions.

4.1.6. Working gas

Multiple different working gases (such as air, oxygen, nitrogen and helium) were used for CAP disinfection by other authors. Hertwig *et al* found stronger inactivation of *B. subtilis* and *B. atrophaeus* spores when nitrogen (N_2) was used as a working gas instead of air [87]. Interestingly, they found no direct correlation between the presence of ozone, ROS, RNS, and the inactivation outcome. Treatments with air, oxygen and CO_2 produced roughly the same *Bacillus* spore inactivation. In contrast, Niemiera reached higher inactivation of *Salmonella* and *E. coli* on almonds with an (indirect) air plasma compared to a nitrogen plasma [106]. Laroussi *et al* indirectly treated *Bacillus* spores with either a pure helium, helium/oxygen (97/3%) or air plasma [107]. The air plasma inactivated the spores more than 20 times faster than the other gas compositions. Wannicke *et al* demonstrated effective inactivation of *B. atrophaeus* spores on seed surfaces by exposing them to plasma-treated air. This air likely contained NO_x species, but low levels of ions, electrons and UV, all of which will disappear before reaching the seed surface [86]. Notably, ozone concentrations were likely very low under their experimental conditions, due to the high plasma temperature (4000 K). Muto and Hayashi showed that denaturation of amino acids such as aspartic and glutamic acid (both present in bacterial spores) was successful in air plasma, but not in oxygen plasma [108]. This indicates that RNS and ROS might act synergistically to achieve disinfection.

Working gases other than ambient air (especially noble gases such as argon [4, 91]) increase operational costs due to the need for controlled gas supply systems and specialized infrastructure. No working gas clearly outperformed ambient air for seed disinfection. Therefore, ambient air remains the most practical and economical choice for CAP disinfection. It was noted that priming effects were stronger in air plasmas compared to oxygen, nitrogen or helium plasmas [109].

Addition of aerosols (H_2O_2, water [110], acetic acid [111] or ethanol [112]) could improve the disinfection in air-based systems. However, for applications such as seed treatment, these additives may have practical drawbacks, namely the need for post-treatment drying, potential non-compliance with food safety regulations and increased costs. Moreover, condensation on the electrodes or the dielectric barrier can disrupt CAP generation by distorting the electric field, impairing the microdischarge formation and accelerating material degradation [22]. Finally, spores may be more resistant to RONS when immersed in water droplets or films [78].

4.1.7. Deeper understanding of inactivation mechanisms

A variety of microbial inactivation mechanisms have been proposed [97]. Among these, oxidation of cell walls, membranes, proteins and nucleic acids is frequently identified as dominant pathway [97, 113]. In our module, oxidation is indeed the most likely inactivation mechanism, as other mechanisms (such as ion etching or electroporation due to PEFs) could be reasonably excluded. For a broader overview of inactivation mechanisms, we refer to the excellent review of Waskow *et al* [16].

Bacterial and particularly fungal spores are widely seen as the most CAP-resistant microbial forms [1, 13]. Their high resistance is linked to minimal metabolic activity and presence of protective structures such as multilayered cell walls, melanin and peptidoglycans (see figure 7(b)) [1, 3, 15, 92, 114]. For this reason, we focused on CAP inactivation of spores, which serve as a stringent benchmark for evaluating overall antimicrobial performance.

Numerous studies have documented structural and biochemical changes in spores after CAP exposure, even by indirect treatments. Hojnik *et al* observed craters in *A. flavus* spores treated indirectly, 5 mm below the discharge electrodes [78]. Similarly, Suwannarat *et al* found cell leakage, pigment loss and surface roughening in *A. brassicicola* spores on seeds placed 5 mm below the discharge electrode [4]. Wang *et al* showed leakage of proteins and DNA from *Alicyclobacillus contaminans* spores, accompanied by a strong reduction in intracellular ATP and cell rupture [115]. Noh *et al* showed a pronounced shrinkage of *Cordyceps pruinosa* spores following direct plasma jet treatment, indicating membrane leakage [116]. They also found elevated intracellular ROS levels and signs of DNA damage in treated spores. Comparable shrinkage and surface erosion were observed by Butscher *et al* in *G. stearothermophilus* spores subjected to an argon CAP treatment [88]. Other studies report shrinking, roughening and clustering of *B. subtilis* spores in a low-pressure direct plasma treatment [104, 117]. Clustering is also described for *Aspergillus parasiticus, A. flavus* and *A. contaminans* spores [103, 115]. This aggregation behaviour has been attributed to an increase in spore surface hydrophilicity induced by CAP exposure [115]. This may also limit the adherence of spores onto hydrophobic seed surfaces. In line with this, Fan *et al* showed a near-complete disappearance of microorganisms from the surface of treated seeds [80]. Spores of *B. cereus* were found to change their water uptake after plasma treatment due to membrane damage [15].

CAP-induced chemical and physiological changes have also been found in fungal mycelia. Šimončicová *et al* reported cell wall desiccation and polysaccharide oxidation in *A. flavus* mycelium exposed to CAP [118]. They found high levels of intracellular antioxidant enzymes, likely reflecting the influx of RONS, through the increasingly permeable fungal cell structures, along with evidence of DNA degradation.

It should be reiterated that the disinfection capability of CAP depends on the type of microorganism [5, 106, 118] and may even differ between per strain [99].

Table 5. Powering parameters (waveform, voltage, frequency) of several studies using a DBD to inactivate bacterial/fungal spores. WG: Working gas. V: Closed air volume of setup. * Calculated based on the dimensions provided by the authors. ** AC frequency while operating in burst mode.

Authors	Type	kV_{pp}	kHz	WG	P_{dens} ($W\ cm^{-2}$)	V (cm^3)	$[O_3]_{max}$ (ppm)
Suwannarat et al [4]	AC	14	1	Ar/Air	1.000	6	?
Klämpfl et al [90]	AC	10	1	Air	0.035	142	?
Beyrer et al [89]	AC	17.5	10	Air	0.180	24	?
Fan et al [80]	Pulsed	22	0.3	Air	0.134*	160	?
Zhang and Wang [117]	Pulsed	44	0.6	Air	0.553*	20	?
Waskow et al [120]	AC	8	10**	Air	0.070	2800	160
Hojnik et al [78]	AC	5-10	40	Air	0.790	39	650
Rotondo et al [121]	AC	20.7	5**	Air	0.289*	1.5	2375
This study	Pulsed	3	0.5	Air	0.009	400	1841
		4			0.024		2399

4.1.8. DBD powering: pulsed vs AC

Pulsed powering might be beneficial for seed disinfection compared conventional AC powering [88]. Short pulses create higher RONS concentrations, while simultaneously limiting heat production [119]. The most energy efficient disinfection was achieved using pulsed, indirect CAP treatment with a moderate V_p for a longer duration. Table 5 shows that pulsed powering, in combination with an optimized DBD, could achieve very high ozone concentrations in comparatively large volumes, at lower power densities compared to other setups.

4.2. DBD performance

Our wire-plate DBD consists of a 7 m-long discharge electrode, positioned a fraction above a thin Gorilla glass barrier. As noted by Kogelschatz *et al*, pulsed CAP systems require sufficiently long electrodes to facilitate simultaneous formation of multiple microdischarges [122]. This was the case in our setup, where microdischarges were observed over a total length of 14 m (see figure 3). A long electrode could also mitigate local heat generation [123]. In our DBD, microdischarges propagated several millimetres over the dielectric surface on both sides of the discharge wire.

Several benefits of this wire-plate DBD could be identified. First, the wire is mechanically robust and resistant to oxidation. Its mechanical strength allows for a small diameter which magnifies the local electric field. This yields several advantages: faster streamer head formation, higher streamer density, improved plasma uniformity [124, 125], increased ionic wind speed [126] and enhanced ozone production [127]. The local electric field is further amplified by the thin dielectric barrier ($d_d = 0.4$ mm) and narrow air gap ($d_g \sim 20\ \mu$m). Together, these features produced a relatively high conduction current (and thus RONS) at low onset voltages ($V_{br} < 2$ kV).

Second, the DBD has a low capacitance ($C_{cell} = 260$ pF). This is caused by the small effective electrode area introduced by the thin wire (area A becomes small in the capacitance equation equation (4)):

$$C = \frac{\varepsilon_0 \cdot \varepsilon_r \cdot A}{d_d}. \tag{4}$$

This small capacitance lowers the pulse rise time, and a shorter rise time increases the conduction current. As a result, microdischarges over a length of 14 m could be produced by a single solid-state push-pull switch. This might benefit industrial implementation, as these switches are reliable and durable compared to other power circuits [128, 129]. The low capacitance extends the operating range of the switch, which is limited by a maximum power ($P_{d,max}$) of 20 W in our case. This follows from equation (5) [58]:

$$P_{d,max} = V_{DC}^2 \cdot \mathrm{PRF} \cdot (C_{cell} + C_{coax} + C_{switch}) \tag{5}$$

where $C_{coax} = 28$ pF and $C_{switch} = 140$ pF.

Third, a low breakdown voltage of enables the use of low-cost switches, as these switches become more expensive for higher voltage ratings. Furthermore, it eliminates the need for noble gas admixtures (e.g. argon) to lower the breakdown voltage [91]. A low V_{br} also lowers heat formation, since less energy is dissipated in the dielectric barrier. For comparison, other authors reached gas temperatures of 30 [89], 57 [18], 70 (with active cooling [87]), 85 [91], 90 [103] and 100 °C [130], whereas we measured a maximum gas temperature of only 28 °C. This indicates that the treatment intensity could be further increased (by increasing V_p, PRF and/or t_{treat}) without risking thermal seed damage [18].

No reflections were detected in the voltage pulse shape [20, 131]. This likely results from the low discharge electrode resistance, achieved by adding two bypass wires to connect the parallel discharge wires (see figure S1). It reduced the resistance >10 times to 10 Ω. Additionally, a thin dielectric barrier lowers the impedance and further suppresses reflections [132]. Other benefits of the bypass wires are lower thermal losses, improved plasma uniformity, and faster charging and discharging of the DBDs capacitive component.

Our DBD is scalable, low-cost (∼ 150 €) and easy to clean. While 300 seeds were treated per experiment, the reactor could contain >10 000 seeds (±50 g) per treatment. However, the disinfection efficacy should then be re-examined. Multiple of these reactors could operate in parallel to treat seeds on an industrial scale, which implies 100 kg h^{-1}. This could be achieved by covering an area of 80 m^2 with these reactors. As ten layers of reactors would easily fit within 1 m of height, a cabinet of 4 × 2 × 1 m^3 could theoretically contain this treatment area. In a 45 min treatment, the power use of the DC supply was 26.5 kJ and that of the switch 9.7 kJ. This amounts to an energy use of 0.01 kWh, which is quite low. For comparison, heating one litre of water from 20 to 60 °C in half an hour (used for thermal seed disinfection) costs 0.04 kWh.

Ultem PEI barriers showed material degradation, while muscovite mica, alumina and semi-resistive C-UHMWPE barriers failed rapidly due to dielectric breakdown. Surface charging was noticed on Corning Willow glass and Gorilla glass barriers, leading to a gradual decrease in current and electrical efficiency. Furthermore, polymer barriers may become more hydrophylic following CAP exposure [68, 70].

The use of short pulses resulted in a duty cycle of only 0.1%. The DBD was operated for >15 h in total. No wire degradation was observed: the VI-characteristics remained unchanged, the wire retained its gold colour (indicating intact plating) and SEM imaging showed no structural defects (see figure S7). The Gorilla glass barrier generally performed well, and displayed only minor scratches after this prolonged period (see figure S8).

Future improvements to this design may include the attachment of magnets to the flat electrode, which could enhance CAP formation [133]. Crystalline barriers (ceramics/mineral) are recommended, as they appear less prone to degradation and surface charging than polymer barriers. Replacing the SiC-MOSFETs in the switch by faster GaN-MOSFETs may further reduce the pulse rise time.

5. Conclusion

A novel type of wire-plate DBD was developed using gold-plated tungsten wire as discharge electrode and Gorilla glass as dielectric barrier. Through several design optimizations—use of a thin wire, a thin dielectric barrier and a minimal air gap—CAP was formed on both sides of a 7 m-long discharge electrode. The DBD showed a low capacitance and discharge electrode resistance, enabling operation with a single HV push-pull switch. The combination of the optimized DBD design and pulsed powering allowed reliable CAP production over a wide operating range (pulse voltage, frequency and width), while minimizing heat production.

The DBD was applied to treat cabbage and carrot seeds contaminated with pathogenic *A. brassicicola* spores, Xcc and Xhc. It was shown that cabbage seeds (containing *A. brassicicola*, Xcc and native microorganisms) were disinfected by up to 98%–100%. Likewise, carrot seeds (containing Xhc and native microorganisms) were disinfected by up to 63%. The lower efficacy for carrot seeds was attributed to their rougher surface structure. Importantly, no reduction of seedling growth was observed.

Analysis of 4 treatment configurations demonstrated that prolonged RONS exposure is most likely the dominant inactivation mechanism. Other plasma components (accelerated ions, electrons, UV-photons and PEFs) did not contribute markedly. However, we could not identify the individual role of each type of RONS (such as O_3) in this inactivation. This could be a direction for future research. Although disinfection was accelerated at higher pulse voltages, it was found to be more energy efficient, and equally effective, to use longer treatment times at slightly lower voltages.

This work shows that a pulsed wire-plate DBD can produce energy-efficient, low-heat and scalable CAP, suitable for seed disinfection. Further improvements could include the use of faster push-pull switches to enhance CAP generation. Surface charging of the dielectric barrier remains an underreported phenomenon that warrants further study. Such charging may be largely averted by using bipolar instead of unipolar pulses. While DBD technology shows a strong potential for seed disinfection, its efficacy appears to be surface- and microorganism-dependent.

Acknowledgments

We thank Yukun Lian, Ilias Walraven and Kees Kwakernaak for their assistance with SEM and Paul van Nes for his valuable comments after proofreading (all Delft University of Technology). We thank dr Hans Höft (INP Greifswald) for his advice on the electronic measurements. This research is funded by the Delft University of Technology, The Netherlands, under the PowerizeD grant (EU 101096387).

Data availability statement

All data that support the findings of this study are included within the article (and any supplementary files).

Supplementary Materials available at: https://doi.org/10.1088/1361-6463/ae8b00/data1.

Funding

The authors have no conflict of interest to declare. This research is funded by the Delft University of Technology, The Netherlands, under the PowerizeD grant (EU 101096387).

ORCID iDs

L F A Wymenga 0009-0007-7943-538X
J van Turnhout 0000-0003-4375-8615
M Ghaffarian Niasar 0000-0003-1766-8077
H W van Zeijl 0000-0001-5204-1646
W D van Driel 0000-0001-8882-2508
G Q Zhang 0000-0002-8023-5170

References

[1] Maojin T, Zheng Z, Ying H, Yanyan H and Liang Z 2025 Bacterial spore inactivation technology in solid foods: a review *J. Food Prot.* **88** 100479

[2] Savary S, Willocquet L, Pethybridge S J, Esker P, McRoberts N and Nelson A 2019 The global burden of pathogens and pests on major food crops *Nat. Ecol. Evol.* **3** 430–9

[3] Thomma B P H J 2003 Alternaria spp.: from general saprophyte to specific parasite *Mol. Plant Pathol.* **4** 225–36

[4] Suwannarat S, Thammaniphit C and Srisonphan S 2021 Electrohydraulic streamer discharge plasma-enhanced alternaria brassicicola disinfection in seed sterilization *ACS Appl. Mater. Interfaces* **13** 43975–83

[5] Mravlje J, Kobal T, Regvar M, Starič P, Zaplotnik R, Mozetič M and Vogel-Mikuš K 2023 The sensitivity of fungi colonising buckwheat grains to cold plasma is species specific *J. Fungi* **9** 609

[6] Nowicki M, Nowakowska M, Niezgoda A and Kozik E 2012 Alternaria black spot of crucifers: symptoms, importance of disease, and perspectives of resistance breeding *J. Fruit Ornamental Plant Res.* **76** 5–19

[7] Suwannarat S, Tephiruk N, Sunan S, Ruangwong K and Srisonphan S 2024 Disinfection efficacy of electrohydraulic discharge plasma against xanthomonas campestris pv campestris: a sustainable seed treatment approach *ACS Appl. Bio Mater.* **7** 1469–77

[8] Nishioka T, Takai Y, Kawaradani M, Okada K, Tanimoto H, Misawa T and Kusakari S 2014 Seed disinfection effect of atmospheric pressure plasma and low pressure plasma on rhizoctonia solani *Biocontrol Sci.* **19** 99102

[9] Vicente J G and Holub E B 2013 Xanthomonas campestris pv. campestris (cause of black rot of crucifers) in the genomic era is still a worldwide threat to brassica crops *Mol. Plant Pathol.* **14** 2–18

[10] Dupas E, Durand K and Jacques M-A 2023 Analysis of the worldwide diversity of xanthomonas hortorum pv. Carotae, the agent of bacterial blight of carrot, reveals two distinct populations *PhytoFrontiers™* **4** 159–71

[11] Molina-Hernandez J B, Grande-Tovar C D, Neri L, Delgado-Ospina J, Rinaldi M, Cordero-Bueso G A and Chaves-López C 2025 Enhancing postharvest food safety: the essential role of non-thermal technologies in combating fungal contamination and mycotoxins *Front. Microbiol.* **16** 1543716

[12] Jo Y-K, Cho J, Tsai T-C, Staack D, Kang M-H, Roh J-H, Shin D-B, Cromwell W and Gross D 2014 A non-thermal plasma seed treatment method for management of a seedborne fungal pathogen on rice seed *Crop Sci.* **54** 796–803

[13] Hoppanová L and Kryštofová S 2022 Nonthermal plasma effects on fungi: applications, fungal responses, and future perspectives *Int. J. Mol. Sci.* **23** 11592

[14] Waskow A, Avino F, Howling A and Furno I 2021 Entering the plasma agriculture field: an attempt to standardize protocols for plasma treatment of seeds *Plasma Process. Polym.* **19** e2100152

[15] Liao X, Liu D, Xiang Q, Ahn J, Chen S, Ye X and Ding T 2017 Inactivation mechanisms of non-thermal plasma on microbes: a review *Food Control* **75** 83–91

[16] Waskow A, Howling A and Furno I 2021 Mechanisms of plasma-seed treatments as a potential seed processing technology *Front. Phys.* **9** 617345

[17] Morin-Crini N *et al* 2022 Removal of emerging contaminants from wastewater using advanced treatments. A review *Environ. Chem. Lett.* **20** 1333–75
[18] Ussenov Y A, Akildinova A, Kuanbaevich B A, Serikovna K A, Gabdullin M, Dosbolayev M, Daniyarov T and Ramazanov T 2022 The effect of non-thermal atmospheric pressure plasma treatment of wheat seeds on germination parameters and α-amylase enzyme activity *IEEE Trans. Plasma Sci.* **50** 330–40
[19] Brandenburg R, Becker K H and Weltmann K-D 2023 Barrier discharges in science and technology since 2003: a tribute and update *Plasma Chem. Plasma Process.* **43** 1303–34
[20] Huiskamp T, Beckers F J C M, Hoeben W F L M, Van Heesch E J M and Pemen A J M 2016 Matching a (sub)nanosecond pulse source to a corona plasma reactor *Plasma Sources Sci. Technol.* **25** 054006
[21] Anuntagool J, Srangsomjit N, Thaweewong P and Alvarez G 2023 A review on dielectric barrier discharge nonthermal plasma generation, factors affecting reactive species, and microbial inactivation *Food Control* **153** 109913
[22] Avino F, Howling A A, Von Allmen M, Waskow A, Ibba L, Han J and Furno I 2023 Surface DBD degradation in humid air, and a hybrid surface-volume DBD for robust plasma operation at high humidity *J. Phys. D: Appl. Phys.* **56** 345201
[23] Moreau E, Bayoda K and Benard N 2021 Streamer propagation and pressure waves produced by a nanosecond pulsed surface sliding discharge: effect of the high-voltage electrode shape *J. Phys. D: Appl. Phys.* **54** 075207
[24] McMaster-Carr Co McMaster-Carr Catalogue (available at: www.mcmaster.com) (Accessed 11 August 2024)
[25] Corning Inc Willow glass safety data sheet (available at: www.mcmaster.com/830oucq/) (Accessed 9 January 2026)
[26] Corning Inc Gorilla glass safety data sheet (available at: www.mcmaster.com/901kuyl/) (Accessed 9 January 2026)
[27] SpecialChem Dielectric strength (available at: www.specialchem.com/plastics/guide/dielectric-strength) (Accessed 11 August 2024)
[28] SpecialChem Polymer water absorption at 24 hours (available at: www.specialchem.com/plastics/guide/water-absorption-24-hours) (Accessed 11 August 2024)
[29] Ozone Solutions Co Ozone compatible materials (available at: https://ozonesolutions.com/blog/ozone-compatible-materials/) (Accessed 11 August 2024)
[30] Oxidation Tech Materials ozone resistance chart (available at: www.oxidationtech.com/blog/materials-ozone-resistance-chart/) (Accessed 11 August 2024)
[31] DuPont de Nemours Inc Kapton data sheet (available at: www.dupont.com/content/dam/electronics/amer/us/en/electronics/public/documents/en/EI-10142_Kapton-Summary-of-Properties.pdf) (Accessed 11 August 2024)
[32] Corning Inc Willow glass fact sheet (available at: www.corning.com/media/worldwide/Innovation/documents/WillowGlass/Corning%20Willow%20Glass%20Fact%20Sheets_August2019.pdf) (Accessed 9 January 2026)
[33] Corning Inc Gorilla glass product sheet (available at: www.corning.com/microsites/csm/gorillaglass/PI_Sheets/2020/Corning%20Gorilla%20Glass%206_PI%20Sheet.pdf) (Accessed 9 January 2026)
[34] Präzisions Glas & Optik EagleXG Technical specifications (available at: www.pgo-online.com/intl/eagle-xg.html) (Accessed 9 January 2026)
[35] Baron Plastics LCC UHMWPE resistance table (available at: https://baronplastics.com/wp-content/uploads/2020/10/PROPRIEDADES-QUIMICAS-ENG-2.pdf) (Accessed 9 January 2026)
[36] Technical Products Inc UHMWPE data sheet (available at: www.technicalproductsinc.com/pdf/Specs/UHMW%20Specs.pdf) (Accessed 9 January 2026)
[37] Asti Sensor Tech ULTEM PEI chemical resistance chart (available at: www.astisensor.com/ultem.pdf) (Accessed 9 January 2026)
[38] PlasticRanger Co Dielectric strength of plastics (available at: https://plasticranger.com/dielectric-strength-of-plastics-electrical-properties-of-plastics/) (Accessed 5 September 2024)
[39] Plastics Intl Chemical resistance chart (available at: www.plasticsintl.com/chemical-resistance-chart/) (Accessed 9 January 2026)
[40] UQG Optics Ltd ITO coated fused quartz data sheet (available at: www.uqgoptics.com/wp-content/uploads/2019/10/ITO-Coated-Fused-Quartz.pdf) (Accessed 9 January 2026)
[41] Masterduct Inc Chemical resistance chart (available at: www.masterduct.com/Portals/0/documents/Masterflex_Chemical Resistance_EN.pdf) (Accessed 9 January 2026)
[42] Bian D, Wu Y, Long C and Lin B 2018 Effects of material degradation on electrical and optical characteristics of surface dielectric barrier discharge *J. Appl. Phys.* **124** 183301
[43] Wei Q, Yang G, Liu G, Jiang H and Zhang T 2018 Effects and mechanism on Kapton film under ozone exposure in a ground near space simulator *Appl. Surf. Sci.* **440** 1083–90
[44] Houser N M, Gimeno L, Hanson R E, Goldhawk T, Simpson T and Lavoie P 2013 Microfabrication of dielectric barrier discharge plasma actuators for flow control *Sens. Actuators A* **201** 101–4
[45] Kim J, Park S and Choe W 2021 Surface plasma with an inkjet-printed patterned electrode for low-temperature applications *Sci. Rep.* **11** 12206
[46] Kim J, Kim S-J, Lee Y-N, Kim I-T and Cho G 2018 Discharge characteristics and plasma erosion of various dielectric materials in the dielectric barrier discharges *Appl. Sci.* **8** 1294
[47] Selivonin I and Moralev I 2020 Microdischarges properties in sDBD: the role of the exposed electrode oxidation *Plasma Sources Sci. Technol.* **30** 035005
[48] Pons J, Oukacine L, Moreau E and Tatibouët J-M 2008 Observation of dielectric degradation after surface dielectric barrier discharge operation in air at atmospheric pressure *IEEE Trans. Plasma Sci.* **36** 1342–3
[49] Ma X, Wang Y, Chen L, Hu L, Wang W, Zhang X and Liu C 2021 Silicon nanowires: the promoter of performance improvement of microplasma in a microcavity array device *Plasma Sources Sci. Technol.* **30** 025010
[50] Francke K-P, Rudolph R and Miessner H 2003 Design and operating characteristics of a simple and reliable DBD reactor for use with atmospheric air *Plasma Chem. Plasma Process.* **23** 47–57
[51] Cheng L, Zhitao Z, Xiaofeng Z and Yan Y 2006 A study of the aging of a-Al_2O_3 dielectric material in DBD plasma *Plasma Sci. Technol.* **8** 693–6
[52] Ito Y, Sakai O and Tachibana K 2010 Measurement of electron density in a microdischarge-integrated device operated in nitrogen at atmospheric pressure using a millimetre-wave transmission method *Plasma Sources Sci. Technol.* **19** 025006
[53] Koo I G, Cho J H, Choi M Y and Lee W M 2007 Room-temperature slot microplasma in atmospheric pressure air between cylindrical electrodes with a nanoporous alumina dielectric *Appl. Phys. Lett.* **91** 041502
[54] Kim M H, Cho J H, Park S J and Eden J G 2017 Modular and efficient ozone systems based on massively parallel chemical processing in microchannel plasma arrays: performance and commercialization *Eur. Phys. J.* **226** 2923–44

[55] Kawasaki T 2009 Basic characteristics of dielectric barrier discharge reactor using anodic porous alumina for NO_x removal *J. Surf. Finish. Soc. Japan* **60** 174–8
[56] Laroussi M, Member S, Alexeff I, Paul Richardson J, Dyer F F, Laroussi M, Richardson J P and Dyer F F 2002 The resistive barrier discharge *IEEE Trans. Plasma Sci.* **30** 158
[57] Liu Y, Yan H, Fan Z, Guo H and Ren C 2017 Influence of residual charge on repetitively nanosecond pulsed dielectric barrier discharges in atmospheric air *Phys. Plasmas* **24** 113514
[58] Behlke GmbH 2023 High voltage push-pull switching units, GHTS series data sheet (available at: www.behlke.com/pdf/ghts.pdf) (Accessed 14 January 2026)
[59] Campbell R 1968 An electron microscope study of spore structure and development in alternaria brassicicola *Microbiology* **54** 381–92
[60] Campbell R 1969 Further electron microscope studies of the conidium of alternaria brassicicola *Arch. Mikrobiol.* **69** 60–68
[61] Sokolova M V, Voevodin V V, Malakhov J I, Aleksandrov N L, Anokhin E M and Soloviev V R 2019 Barrier properties influence on the surface dielectric barrier discharge driven by single voltage pulses of different duration *J. Phys. D: Appl. Phys.* **52** 324001
[62] Gibalov V I and Pietsch G J 2000 The development of dielectric barrier discharges in gas gaps and on surfaces *J. Phys. D: Appl. Phys.* **33** 2618–36
[63] Haacke M, Humpert C and Pietsch G J 2002 Influence of field strength and energy distribution of different barrier discharge arrangements on ozone generation *Ozone* **24** 193–201
[64] Jiang H and Shao T 2023 Surface dielectric barrier discharge driven by nanosecond pulses *Pulsed Discharge Plasmas* ed T Shao and C Zhang (Springer) pp 635–72
[65] Elchaninov V M, Shemet M V and Malashin M V 2017 Dielectric barrier discharge excited by unipolar pulse voltage in sub-millimetric air gaps *IEEE Conf. of Russian Young Researchers in Electrical and Electronic Engineering (Eiconrus)* (St. Petersburg Electrotechnical University "LETI" ; National Research University of Electronic Technology "MIET") pp 1135–7
[66] Schweiger C *et al* 2022 Fast silicon carbide MOSFET based high-voltage push-pull switch for charge state separation of highly charged ions with a Bradbury-Nielsen gate *Rev. Sci. Instrum.* **93** 094702
[67] Kriegseis J, Möller B, Grundmann S and Tropea C 2011 Capacitance and power consumption quantification of dielectric barrier discharge (DBD) plasma actuators *J. Electrostat.* **69** 302–12
[68] Opaits D F, Shneider M N, Miles R B, Likhanskii A V and MacHeret S O 2008 Surface charge in dielectric barrier discharge plasma actuators *Phys. Plasmas* **15** 073505
[69] Wegener M, Wirges W, Paajanen M and Gerhard R 2007 Charging behavior and thermal stability of porous and non-porous polytetrafluoroethylene (PTFE) electrets *2007 Annual Report Conf. on Electrical Insulation and Dielectric Phenomena* pp 449–52
[70] Labiod S, Ziari Z, Benterrouche L and Sahli S 2022 Surface potential decay evolution of polypropylene films treated by dielectric barrier discharge in atmospheric air *2022 2nd Int. Conf. on Advanced Electrical Engineering, ICAEE 2022* (Institute of Electrical and Electronics Engineers Inc)
[71] Zhang B and Zhang G 2017 Interpretation of the surface charge decay kinetics on insulators with different neutralization mechanisms *J. Appl. Phys.* **121** 105105
[72] Pipa A V, Hoder T, Koskulics J, Schmidt M and Brandenburg R 2012 Experimental determination of dielectric barrier discharge capacitance *Rev. Sci. Instrum.* **83** 075111
[73] Yuan D, Wang Z, Ding C, He Y, Whiddon R and Cen K 2016 Ozone production in parallel multichannel dielectric barrier discharge from oxygen and air: the influence of gas pressure *J. Phys. D: Appl. Phys.* **49** 455203
[74] Park S, Kim J, Lee H, Han D, Park S, Kim S B and Choe W 2021 Nonheating ozone suppression in pulsed air discharges: role of pulse duration and repetition rate *J. Phys. D: Appl. Phys.* **54** 394003
[75] Cimerman R and Hensel K 2023 Multi-hollow surface dielectric barrier discharge: production of gaseous species under various air flow rates and relative humidities *Plasma Chem. Plasma Process.* **43** 1411–33
[76] Jodzis S and Baran K 2022 The influence of gas temperature on ozone generation and decomposition in ozone generator. How is ozone decomposed? *Vacuum* **195** 110647
[77] Laika J, Viteritti E, Molina-Hernandez J B, Sergi M, Neri L, Laurita R, Tappi S, Ricci A and Chaves-López C 2024 Efficiency of cold atmospheric plasma under ozone (O_3) and nitrogen oxide (NO_x) regimes on the degradation of aflatoxins and ochratoxin A in solid state and in spiked pistachio kernels *Food Control* **159** 110286
[78] Hojnik N, Modic M, Ni Y, Filipič G, Cvelbar U and Walsh J L 2019 Effective fungal spore inactivation with an environmentally friendly approach based on atmospheric pressure air plasma *Environ. Sci. Technol.* **53** 1893–904
[79] Timmermann E, Prehn F, Schmidt M, Höft H, Brandenburg R and Kettlitz M 2018 Indoor air purification by dielectric barrier discharge combined with ionic wind: physical and microbiological investigations *J. Phys. D: Appl. Phys.* **51** 164003
[80] Fan T, Chen Y, Zhang N, Wang Y, Wang X, Chang D and Yang K 2023 Nanosecond pulsed atmospheric-pressure plasma enhanced the germination of melon (Cucumis melo L.) seeds *Plasma Chem. Plasma Process.* **43** 1149–67
[81] August J, Dufour T and Bailly C 2023 Release of Arabidopsis seed dormancy by cold atmospheric plasma relies on cytoplasmic glass transition *J. Phys. D: Appl. Phys.* **56** 415202
[82] Ďurčányová S, Slováková Ĺ, Klas M, Tomeková J, Ďurina P, Stupavská M, Kováčik D and Zahoranová A 2023 Efficacy comparison of three atmospheric pressure plasma sources for soybean seed treatment: plasma characteristics, seed properties, germination *Plasma Chem. Plasma Process.* **43** 1863–85
[83] Waskow A, Butscher D, Oberbossel G, Klöti D, Rudolf von Rohr P, Büttner-Mainik A, Drissner D and Schuppler M 2021 Low-energy electron beam has severe impact on seedling development compared to cold atmospheric pressure plasma *Sci. Rep.* **11** 16373
[84] Šrámková P, Kostoláni D, Kyzek S, Bathoova M, Ďurčányová S, Stupavská M, Gálová E, Zahoranová A and Švubová R 2025 Extending shelf life: cold plasma as a tool to preserve long-term germination potential of pea seeds *Sci. Rep.* **15** 35001
[85] Nacheva L, Milusheva S, Marinova P, Dimitrova N and Benova E 2024 Cold atmospheric plasma (CAP) treatment of *in vitro* cultivated plum plantlets—a possible way to improve growth and inactivate plum pox virus (PPV) *Processes* **12** 1837
[86] Wannicke N, Wagner R, Stachowiak J, Nishime T M C, Ehlbeck J, Weltmann K-D and Brust H 2020 Efficiency of plasma-processed air for biological decontamination of crop seeds on the premise of unimpaired seed germination *Plasma Process. Polym.* **18** e2000207
[87] Hertwig C, Reineke K, Rauh C and Schlüter O 2017 Factors involved in Bacillus spore's resistance to cold atmospheric pressure plasma *Innov. Food Sci. Emerg. Technol.* **43** 173–81
[88] Butscher D, Zimmermann D, Schuppler M and Rudolf von Rohr P 2016 Plasma inactivation of bacterial endospores on wheat grains and polymeric model substrates in a dielectric barrier discharge *Food Control* **60** 636–45

[89] Beyrer M, Smeu I, Martinet D, Howling A, Pina-Pérez M C and Ellert C 2020 Cold atmospheric plasma inactivation of microbial spores compared on reference surfaces and powder particles *Food Bioprocess Technol.* **13** 827–37

[90] Klämpfl T G, Isbary G, Shimizu T, Li Y-F, Zimmermann J L, Stolz W, Schlegel J, Morfill G E and Schmidt H-U 2012 Cold atmospheric air plasma sterilization against spores and other microorganisms of clinical interest *Appl. Environ. Microbiol.* **78** 5077–82

[91] Butscher D, Van Loon H, Waskow A, Rudolf von Rohr P and Schuppler M 2016 Plasma inactivation of microorganisms on sprout seeds in a dielectric barrier discharge *Int. J. Food Microbiol.* **238** 222–32

[92] Molina-Hernandez J B, Laika J, Peralta-Ruiz Y, Palivala V K, Tappi S, Cappelli F, Ricci A, Neri L and Chaves-López C 2022 Influence of atmospheric cold plasma exposure on naturally present fungal spores and physicochemical characteristics of sun-dried tomatoes (*Solanum lycopersicum* L.) *Foods* **11** 210

[93] Opretzka J, Benedikt J, Awakowicz P, Wunderlich J and Von Keudell A 2007 The role of chemical sputtering during plasma sterilization of Bacillus atrophaeus *J. Phys. D: Appl. Phys.* **40** 2826–30

[94] Schnabel U, Niquet R, Krohmann U, Winter J, Schlüter O, Weltmann K-D and Ehlbeck J 2012 Decontamination of microbiologically contaminated specimen by direct and indirect plasma treatment *Plasma Process. Polym.* **9** 569–75

[95] Hähnel M, Von Woedtke T and Weltmann K-D 2010 Influence of the air humidity on the reduction of bacillus spores in a defined environment at atmospheric pressure using a dielectric barrier surface discharge *Plasma Process. Polym.* **7** 244–9

[96] Ragni L, Berardinelli A, Vannini L, Montanari C, Sirri F, Guerzoni M E and Guarnieri A 2010 Non-thermal atmospheric gas plasma device for surface decontamination of shell eggs *J. Food Eng.* **100** 125–32

[97] Bourke P, Ziuzina D, Han L, Cullen P J and Gilmore B F 2017 Microbiological interactions with cold plasma *J. Appl. Microbiol.* **123** 308–24

[98] Pavlovich M J, Clark D S and Graves D B 2014 Quantification of air plasma chemistry for surface disinfection *Plasma Sources Sci. Technol.* **23** 065036

[99] Salmon A, Stancu G D and Laux C O 2021 Decontamination of endospores by plasma sources on dried surfaces: a review of key parameters and inactivation results *Front. Phys.* **9** 677971

[100] Pérez Pizá M C, Prevosto L, Zilli C, Cejas E, Kelly H and Balestrasse K 2018 Effects of non–thermal plasmas on seed-borne diaporthe/phomopsis complex and germination parameters of soybean seeds *Innov. Food Sci. Emerg. Technol.* **49** 82–91

[101] Plank T, Jalakas A, Aints M, Paris P, Valk F, Viidebaum M and Jõgi I 2014 Ozone generation efficiency as a function of electric field strength in air *J. Phys. D: Appl. Phys.* **47** 335205

[102] Peng B, Jiang N, Liu Z, Yao X, Li J and Wu Y 2022 Discharge dynamics of primary and secondary streamers in a repetitively pulsed surface dielectric barrier discharge *J. Appl. Phys.* **131** 113301

[103] Dasan B G, Mutlu M and Boyaci I H 2016 Decontamination of *Aspergillus flavus* and *Aspergillus parasiticus* spores on hazelnuts via atmospheric pressure fluidized bed plasma reactor *Int. J. Food Microbiol.* **216** 50–59

[104] Yoshino K, Matsumoto H, Iwasaki T, Kinoshita S, Noda K and Iwamori S 2013 Monitoring of sterilization in an oxygen plasma apparatus, employing a quartz crystal microbalance (QCM) method *Vacuum* **93** 84–89

[105] Veerana M, Yu N, Ketya W and Park G 2022 Application of non-thermal plasma to fungal resources *J. Fungi* **8** 102

[106] Niemira B A 2012 Cold plasma reduction of salmonella and Escherichia coli O157: H7 on almonds using ambient pressure gases *J. Food Sci.* **77** M171–5

[107] Laroussi M and Leipold F 2004 Evaluation of the roles of reactive species, heat, and UV radiation in the inactivation of bacterial cells by air plasmas at atmospheric pressure *Int. J. Mass Spectrom.* **233** 81–86

[108] Muto R and Hayashi N 2023 Sterilization characteristics of narrow tubing by nitrogen oxides generated in atmospheric pressure air plasma *Sci. Rep.* **13** 6947

[109] Zhou R, Zhou R, Zhang X, Zhuang J, Yang S, Bazaka K and Ostrikov K K 2016 Effects of atmospheric-pressure N_2, He, air, and O_2 microplasmas on mung bean seed germination and seedling growth *Sci. Rep.* **6** 32603

[110] Zhou Y, Jiang T, Zhang L, Wang S, Zhou R, Cui X and Fang Z 2023 High reactivity and bactericidal effects of plasma-activated mist from hydrogen peroxide solution *Plasma Process. Polym.* **20** e2200140

[111] Kang T, Yim D, Baek K H, Lee Y E, Kim H-J and Jo C 2022 The inactivation efficacy of plasma-activated acetic acid against *Salmonella typhimurium* cells and biofilm *J. Appl. Microbiol.* **133** 3007–19

[112] Li Y Q, Liu J L, Zhao F, Song K, Nie L L, Liu D W and Lu X P 2023 Plasma-activated ethanol solution and it is decontamination effect *High Volt.* **8** 833–40

[113] Lim J-P, Uhm H S and Li S-Z 2007 Influence of oxygen in atmospheric-pressure argon plasma jet on sterilization of *Bacillus atrophaeous* spores *Phys. Plasmas* **14** 093504

[114] Raguse M, Fiebrandt M, Denis B, Stapelmann K, Eichenberger P, Driks A, Eaton P, Awakowicz P and Moeller R 2016 Understanding of the importance of the spore coat structure and pigmentation in the *Bacillus subtilis* spore resistance to low-pressure plasma sterilization *J. Phys. D: Appl. Phys.* **49** 285401

[115] Wang Z, Zhao Q, Gan Y, Fan Q, Hu Z, Wang Z, Cai R, Yue T and Yuan Y 2023 Inactivation of *Alicyclobacillus* contaminans spores by dielectric barrier discharge plasma and its biological mechanism *Innov. Food Sci. Emerg. Technol.* **87** 103415

[116] Noh H, Kim J E, Kim J Y, Kim S H, Han I, Lim J S, Ki S H, Choi E H and Lee G J 2019 Spore viability and cell wall integrity of *Cordyceps pruinosa* treated with an electric shock-free, atmospheric-pressure air plasma jet *Appl. Sci.* **9** 3921

[117] Zhang Y and Wang H 2025 The effect of discharge uniformity on the tailing phenomenon of spore inactivation by cold atmospheric plasma *AIP Adv.* **15** 105108

[118] Šimončicová J *et al* 2018 Cold plasma treatment triggers antioxidative defense system and induces changes in hyphal surface and subcellular structures of *Aspergillus flavus Appl. Microbiol. Biotechnol.* **102** 6647–58

[119] Williamson J M, Trump D D, Bletzinger P and Ganguly B N 2006 Comparison of high-voltage ac and pulsed operation of a surface dielectric barrier discharge *J. Phys. D: Appl. Phys.* **39** 4400–6

[120] Waskow A, Ibba L, Leftley M, Howling A, Ambrico P F and Furno I 2021 An *in situ* FTIR study of DBD plasma parameters for accelerated germination of arabidopsis thaliana seeds *Int. J. Mol. Sci.* **22** 11540

[121] Rotondo P R, Rotolo C, Hoffer P, Fujera J, Prukner V, Faretra F, De Miccolis Angelini R M and Šimek M 2025 Decontaminant activity of volume dielectric barrier discharge against *Fusarium* spp. on barley seeds *Sci. Rep.* **15** 28106

[122] Kogelschatz U, Eliasson B and Egli W 1997 Dielectric barrier discharges. Principle and applications *J. Phys. IV Proc.* **C4** 4–47

[123] Malik M A, Schoenbach K H, Abdel-Fattah T M, Heller R and Jiang C 2016 Low cost compact nanosecond pulsed plasma system for environmental and biomedical applications *Plasma Chem. Plasma Process.* **37** 59–76

[124] Murooka Y, Takada T and Hiddaka K 2001 Nanosecond surface discharge and charge density evaluation part I: review and experiments *IEEE Electr. Insul. Mag.* **17** 6–16

[125] Wang D and Namihira T 2020 Nanosecond pulsed streamer discharges: II. Physics, discharge characterization and plasma processing *Plasma Sources Sci. Technol.* **29** 023001

[126] Li J-Q, Yan H-J, Li T, Yu S-Q, Fan J-W and Song J 2023 Surface charge characteristics in surface dielectric barrier discharge actuators with thin cylindrical exposed electrode *J. Appl. Phys.* **133** 063301

[127] Huiskamp T, Subramanian S, Gururajan V, Schroeder W P, Schroeder C A, Gundersen M A and Cronin S B 2020 Boosting the energy efficiency of a nanosecond pulsed corona plasma system with a multiple-wire plasma reactor *IEEE Trans. Plasma Sci.* **48** 245–57

[128] Huiskamp T, Van Heesch E and Pemen A 2023 Pulsed power generators *Pulsed Discharge Plasmas* ed T Shao and C Zhang (Springer) pp 3–44

[129] Zhuge Y, Liang J, Fu M, Long T and Wang H 2024 Comprehensive overview of power electronics intensive solutions for high-voltage pulse generators *IEEE Open J. Power Electron.* **5** 21–40

[130] Butscher D, Schlup T, Roth C, Müller-Fischer N, Gantenbein-Demarchi C and Rudolf Von Rohr P 2015 Inactivation of microorganisms on granular materials: reduction of *Bacillus amyloliquefaciens* endospores on wheat grains in a low pressure plasma circulating fluidized bed reactor *J. Food Eng.* **159** 48–56

[131] Pipa A V, Hoder T and Brandenburg R 2013 On the role of capacitance determination accuracy for the electrical characterization of pulsed driven dielectric barrier discharges *Contrib. Plasma Phys.* **53** 469–80

[132] Correale G, Avallone F and Starikovskiy A Y 2016 Experimental method to quantify the efficiency of the first two operational stages of nanosecond dielectric barrier discharge plasma actuators *J. Phys. D: Appl. Phys.* **49** 505201

[133] Guo H, Xu Y, Wang Y and Ren C 2020 Experimental study on the effects of airflow, magnetic field and combination of airflow with magnetic field on nanosecond pulsed dielectric barrier discharge in atmospheric air *Phys. Plasmas* **27** 023519